

1 **A Tad-like apparatus is required for contact-dependent prey killing in predatory social**
2 **bacteria**

3
4
5
6
7

Sofiene Seef^{1*}, Julien Herrou^{1*}, Paul de Boissier², Laetitia My¹, Gael Brasseur¹, Donovan Robert¹,
Rikesh Jain^{1,2}, Romain Mercier¹, Eric Cascales³, Bianca Habermann², Tâm Mignot¹

8 Affiliations:

9 ¹ Aix-Marseille Université - CNRS UMR 7283, Institut de Microbiologie de la Méditerranée and
10 Turing Center for Living Systems.

11 ² Aix-Marseille Université - CNRS UMR 7288, Institut de Biologie du Développement de
12 Marseille and Turing Center for Living Systems.

13 ³ Aix-Marseille Université - CNRS UMR 7255, Institut de Microbiologie de la Méditerranée.

14 *denotes equal contribution

15 Correspondence: tmignot@imm.cnrs.fr

16

17 **Summary:**

18 *Myxococcus xanthus*, a soil bacterium, predaes collectively using motility to invade prey colonies.
19 Prey lysis is mostly thought to rely on secreted factors, cocktails of antibiotics and enzymes, and
20 perhaps a mysterious contact-dependent mechanism. In this study we show that the coupling of A-
21 motility and contact-dependent killing is the central predatory mechanism driving effective prey
22 colony invasion and consumption. At the molecular level, contact-dependent killing is driven by a
23 newly discovered type IV filament-like machinery (Kil) that both promotes motility arrest and
24 prey cell plasmolysis. In this process, Kil proteins assemble at the predator-prey contact site,
25 suggesting that they allow tight contact with prey cells for their intoxication. Kil-like systems form
26 a new class of Tad-like machineries in predatory bacteria, suggesting a conserved function in
27 predator-prey interactions. This study further reveals a novel cell-cell interaction function for
28 bacterial pili-like assemblages.

29

30

31 Bacterial predators have evolved strategies to consume other microbes as a nutrient source. Despite
32 the suspected importance of predation on microbial ecology¹, a limited number of bacterial species
33 are currently reported as predatory. Amongst them, obligate intracellular predators collectively
34 known as BALOs (*eg Bdellovibrio bacteriovorus*)¹ penetrate their bacterial prey cell wall and
35 multiply in the periplasm escaping and killing the host bacteria². Quite differently, facultative
36 predators (meaning that they can be cultured in absence of prey if nutrient media are provided, *ie*
37 *Myxococcus*, *Lysobacter* and *Herpetosiphon*¹) attack their preys extracellularly, presumably by
38 secreting antimicrobial substances and digesting the resulting products. Among these organisms
39 and studied here, *Myxococcus xanthus*, a delta-proteobacterium, is of particular interest because it

40 uses large-scale collective movements to attack prey bacteria in a so-called “wolf-pack”
41 mechanism³.

42 A tremendous body of work describes how *Myxococcus* cells move and respond to signals
43 in pure culture⁴. In contrast, mechanistic studies of the predatory cycle have been limited.
44 Currently, it is considered that coordinated group movements allow *Myxococcus* cells to invade
45 prey colonies and consume them via the secretion of a number of diffusible factors, extracellular
46 enzymes, antibiotics and outer membrane vesicles^{3,5,6}. While each of these processes could each
47 contribute to predation, evidence for their requirement is still missing³. In addition, *Myxococcus*
48 cells have also been observed to induce prey cell plasmolysis upon contact⁷. While a number of
49 contact-dependent mechanisms could be involved including Type VI secretion⁸ and Outer
50 Membrane Transfer (OME⁹, see below), none have yet been implicated in predation. In this study,
51 we analyzed the importance of motility and contact-dependent killing in the *Myxococcus* predation
52 cycle.

53 To explore these central questions, we first developed a sufficiently resolved imaging assay
54 where the *Myxococcus* predation cycle can be imaged stably at the single cell level over periods
55 of time encompassing several hours with a temporal resolution of seconds. The exact methodology
56 underlying this technique is described in a dedicated manuscript¹⁰; briefly, the system relates
57 predatory patterns observed at the mesoscale with single cell resolution, obtained by zooming in
58 and out on the same microscopy specimen (Figure 1a). Here, we employed it to study how
59 *Myxococcus* cells invade and grow over *Escherichia coli* prey cells during the initial invasion stage
60 (Figure 1a, Movie S1).

61
62 ***A-motility is required for prey colony invasion.*** Although the function of motility in prey invasion
63 is generally accepted, *Myxococcus xanthus* possesses two independent motility systems and the
64 relative contribution of each system to the invasion process is unknown. Social (S)-motility is a
65 form of bacterial “twitching” motility that uses so-called Type IV pili (Tfp) acting at the bacterial
66 pole¹¹. In this process, polymerized Tfps act like “grappling hooks” that retract and pull the cell
67 forward. S-motility promotes the coordinated movements of *Myxococcus* cells within large cell
68 groups due to interaction with a self-secreted extracellular matrix formed of Exo-Polysaccharide
69 (EPS)¹². A(Adventurous)-motility promotes the movement of *Myxococcus* single cells at the
70 colony edges. A-motility is driven by a mobile cell-envelope motor complex (named Agl-Glt) that
71 traffics in helical trajectories along the cell axis, driving rotational propulsion of the cell when it
72 becomes tethered to the underlying surface at so-called bacterial Focal Adhesions (bFAs)¹³. We
73 tested the relative contribution of each motility system to prey invasion by comparing the relative
74 predatory performances of WT, A⁺S⁻(*pilA*¹⁴) and A⁻(*aglQ*¹⁴) S⁺. Interestingly, although A⁺S⁻ cells
75 were defective in the late developmental steps (fruiting body formation), they were still proficient
76 at prey invasion (Figure 1b). On the contrary, the A⁻S⁺ strain was very defective at prey colony
77 invasion (Figure 1c). Zooming at the prey colony border, it was apparent that the A⁻S⁺ cells were
78 able to expand and contact the prey colony, but they were unable to penetrate it efficiently,
79 suggesting that Type IV pili on their own are not sufficient for invasion (Figure 1c, movie S2).

80 Conversely, A-motile cells were observed to penetrate the tightly-knitted *E. coli* colony with single
81 *Myxococcus* cells moving into the prey colony, followed by larger cell groups (Figure 1a a1-a2).
82 Thus, A-motility is the main driver of prey invasion.

83

84 ***A-motile cells kill prey cells upon contact.*** To further determine how A-motility promotes prey
85 colony invasion we shot single cell time-lapse movies of the invasion process. First, we localized
86 a bFA marker, the AglZ protein¹⁵ fused to Neon-Green (AglZ-NG) in *Myxococcus* cells as they
87 penetrate the prey colony. AglZ-NG binds to the cytoplasmic face of the Agl-Glt complex and has
88 long been used as a bFA localization marker; it generally forms fixed fluorescent clusters on the
89 ventral side of the cell that retain fixed positions in gliding cells¹⁵. As *Myxococcus* cells invaded
90 prey colonies, they often formed “arrow-shaped” cell groups, in which the cells within the arrow
91 assembled focal adhesions (Figure 2a, Movie S3). Remarkably, *E. coli* cells lysed in contact with
92 the *Myxococcus* cells, suggesting that the invading A-motile cells carry a prey toxic activity
93 (Figure 2a). To observe this activity directly, we set up a *Myxococcus-E. coli* interaction
94 microscopy assay where predator-prey interactions can be easily studied, isolated from a larger
95 multicellular context (Methods). In this system, A-motile *Myxococcus* cells were observed to mark
96 a pause and disassemble bFAs when contacting *E. coli* cells (Figure 2b, Movie S4, further
97 quantified below); this pause was invariably followed by the rapid death of *E. coli*, as detected by
98 the instantaneous dispersal of a cytosolic fluorescent protein (mCherry/GFP, Figure 2b-2c,
99 observed in n=20 cells). This observation is entirely consistent with a recent study that reported
100 *Myxococcus*-induced *E. coli* plasmolysis upon contact⁷. To further explore this process, we mixed
101 *Myxococcus* cells with *E. coli* cells in which peptidoglycan (PG) had been labeled by fluorescent
102 D-amino Acids (TADA¹³). TADA is covalently incorporated into the PG pentapeptide backbone
103 and it does not diffuse laterally¹⁶. We first observed contraction of the *E. coli* cytosolic dense region
104 at the pole by phase contrast (Figure 2d), which was followed by the appearance of a dark area in
105 the PG TADA staining exactly at the predator-prey contact site (Figure 2d). It is unlikely that this
106 dark area forms due to the new incorporation of unlabeled prey PG, because it was detected
107 immediately upon prey cell death and propagated bi-directionally afterwards (Figure 2d-e). Thus,
108 these observations suggest that upon contact, *Myxococcus* breaches a hole in the *E. coli* PG, which
109 provokes cell lysis due to loss of turgor pressure and hyper osmotic shock⁷. The bi-directional
110 propagation of PG hydrolysis (as detected by loss of TADA signal) suggests that PG hydrolysis
111 could be driven by the activity of PG hydrolase(s) disseminating from the predator-prey contact
112 site.

113

114 ***A predicted Tad-pilus is required for contact-dependent killing.*** We next aimed to identify the
115 molecular system that underlies contact-dependent killing. Direct transplantation of A⁻S⁻ (*aglQ*
116 *pilA*) in *E. coli* prey colonies still exhibit contact-dependent killing (Figure S1a), demonstrating
117 that the killing activity is not carried by the motility complexes themselves. *Myxococcus xanthus*
118 also expresses a functional Type VI secretion system (T6SS), which appears to act as a factor
119 modulating population homeostasis and mediating Kin discrimination between *M. xanthus*

120 strains^{8,17}. A T6SS deletion strain ($\Delta t6ss$) had no observable defect in contact-dependent killing of
121 prey cells (Figure S1b). In addition, the *Myxococcus* T6SS assembled in a prey-independent
122 manner as observed using a functional VipA-GFP strain that marks the T6SS contractile sheath¹⁸
123 (Figure S1c-e), confirming that T6SS is not involved in predatory killing.

124 To identify the contact-dependent killing mechanism, we designed an assay where contact-
125 dependent killing can be directly monitored in liquid cultures and observed via a simple
126 colorimetric assay. In this system, the lysis of *E. coli* cells can be directly monitored when
127 intracellular β -galactosidase is released in buffer containing ChloroPhenol Red- β -D-
128 Galactopyranoside (CPRG), which acts as a substrate for the enzyme and generates a dark red
129 hydrolysis reaction product¹⁹. Indeed, while *Myxococcus* or *E. coli* cells incubated alone did not
130 produce color during a 120-hour incubation, their mixing produced red color indicative of *E. coli*
131 lysis after 24 h (Figure S2). In this assay, motility and *t6SS* mutants were also able to lyse *E. coli*
132 cells (Figure S2). CPRG hydrolysis was not detected when *Myxococcus* and *E. coli* were separated
133 by a semi-permeable membrane that allows diffusion of soluble molecules, showing that the assay
134 reports contact-dependent killing (Figure S2). We thus used this assay to screen for mutations in
135 predicted cell-envelope complexes, in which contact-dependent killing is abolished. Doing so, we
136 identified two genetic regions, the MXAN_3102-3108 and the MXAN_4648-4661 in which
137 genetic deletions profoundly affected contact-dependent killing in liquid cultures (Figure 3).

138 Functional annotations indicate that both genetic regions carry a complementary set of
139 genes encoding proteins that assemble a so-called **Tight adherence** (Tad) pilus. Bacterial Tad pili
140 are members of the type IV filament superfamily (also including Type IV pili, a and b types, and
141 Type II secretion systems) and extrude polymeric pilin filaments assembled via inner membrane
142 associated motors through an OM secretin²⁰. Tad pili have been generally involved in bacterial
143 adhesion and more recently, in contact-dependent regulation of adhesion²¹. Within the
144 MXAN_3102-3108 cluster, genes with annotated functions encode a predicted pre-pilin peptidase
145 (CpaA and renamed KilA) following the *Caulobacter crescentus* Tad pilus encoding *cpa* genes
146 nomenclature), a secretin homolog (CpaC/KilC) and a cytoplasmic hexameric ATPase
147 (CpaF/KilF) (Figure 3a, Figure S3A-B, Table S1). All the other genes encode proteins of unknown
148 function, with two predicted OM lipoproteins and several proteins containing predicted ForkHead-
149 Associated domains (FHA²², Table S1, see discussion). The second genetic region, MXAN_4648-
150 4661, contains up to 14 predicted open-reading frames of which the only functionally annotated
151 genes encode homologs of the Tad IM platform proteins (CpaG/KilG and CpaH/KilH), OM
152 protein (CpaB/KilB), major pilin (Flp/KilK) and two pseudo-pilin subunits (KilL, M) (Figure 3a,
153 Figure S3c-d, Table S1²⁰). However, the splitting of Tad homologs in distinct genetic clusters is a
154 unique situation²⁰ and asks whether these genes encode proteins involved in the same function.

155 Expression analysis suggests that the cluster 1 and cluster 2 genes are expressed together
156 and induced in starvation conditions (Figure S4a²³). We systematically deleted all the predicted
157 Tad components in cluster 1 and 2 alone or in combination and measured the ability of each mutant
158 to lyse *E. coli* in the CPRG colorimetric assay (Figure 3b). All the predicted core genes, IM
159 platform, OM secretin and associated CpaB homolog are essential for prey lysis, with the

160 exception of the putative pre-pilin peptidase, KilA. Deletion of the genes encoding predicted
161 pseudo-pilins KilL and M did not affect *E. coli* killing; in these conditions, pilin fibers are only
162 partially required because deletion of KilK, the major pilin subunit, reduces the lytic activity
163 significantly but not fully (Figure 3b). We next tested the function of selected *kil* mutants, predicted
164 secretin (KilC), IM platform (KilH and KilG), OM-CpaB homolog (KilB), pilin and pseudopilins
165 (KilK, L, M) in contact-dependent killing at the single cell level. Prey recognition is first revealed
166 by the induction of a motility pause upon prey cell contact (Figure 2). This recognition was
167 severely impaired although not fully in secretin (*kilC*), IM platform protein (*kilG*) and triple pilin
168 ($\Delta kilKMN$) mutants (Figure 3c, ~8% of the contacts led to motility pauses vs ~30% for the WT).
169 In contrast, recognition was not impaired to significant levels in IM platform protein (*kilH*), CpaB-
170 homolog (*kilB*) and pilin (*kilK*) mutants (Figure 3c). The potential basis of this differential impact
171 is further analyzed in the discussion. On the contrary, prey cell plasmolysis was dramatically
172 impacted in all predicted core components (~2% of the contacts led to prey lysis vs ~26% for the
173 WT), the only exception being the single pilin (*kilK*) mutant in which prey cell lysis was reduced
174 but still present (~13%, Figure 3d). Deletion of all three genes encoding pilin-like proteins
175 nevertheless affected in prey cell killing to levels observed in core component mutants. This is not
176 observed to such extent in the CPRG assay, which could be explained by different cell-cell
177 interaction requirements in these two conditions (see Discussion). Given the prominent role of the
178 pilins at the single cell level, the predicted pre-pilin peptidase KilA would have been expected to
179 be essential. However, expression of the *kilA* gene is very low under all tested conditions (Figure
180 S4a). Prepilin peptidases are known to be promiscuous²⁴ and thus another peptidase (ie PilD, the
181 Type IV pilus peptidase²⁵) could also process the Kil-associated pilins. This hypothesis could
182 however not be tested because PilD appears essential for reasons that remain to be determined²⁵.
183 Altogether, the data supports that the proteins from the two clusters function in starvation
184 conditions and that they could make up a Tad-like core structure. This system (Kil) plays a role
185 both in prey cell recognition, regulating motility in contact with prey cells, and prey killing,
186 allowing contact-dependent plasmolysis.

187

188 ***Kil proteins assemble at contact sites and mediate motility regulation and killing.*** To determine
189 how the Kil apparatus mediates these functions, we sought to localize its activity directly upon
190 contact with prey cells. It is difficult to obtain functional fluorescent fusions to Tad core proteins
191 as these proteins insert into the cell envelope and often interact with several partner proteins in
192 high molecular weight membrane complexes²⁰. We thus searched for a potential Kil-associated
193 protein that would tolerate a fluorescent tag. Downstream from *kilF* and likely co-transcribed, the
194 MXAN_3108 gene (*kilD*, Figures 3a, S4a) encodes a predicted cytoplasmic multidomain protein
195 also required for killing and thus functionally associated with the Kil apparatus (Figure 3b). An N-
196 terminal fusion of Neon-Green (NG) to KilD was stably expressed from the native, chromosomal
197 locus (Figure S4b) and proficient for contact-dependent killing. During this process, NG-KilD was
198 diffuse in the cytoplasm but it rapidly formed a fluorescent-bright cluster exactly at a prey contact
199 site (Figure 4a-4b, Movie S5). Cluster formation was invariably followed by a motility pause and

200 cell lysis (Figure 4a-4b). Remarkably, the clusters did not localize to any specific cellular site but
201 they formed where *Myxococcus* cells touched prey cells, assembling up to three clusters for three
202 contact sites (Figure 4a-4b). Cluster formation was correlated to motility arrest and their dispersal
203 coincided with motility resumption (Figure 4a-4b). TADA-labeling of *E. coli* cells indicated that
204 PG holes form exactly at the points where the clusters are formed, showing unambiguously that
205 cluster formation reflects contact-dependent killing (Figure 4c). Using cluster assembly as a proxy
206 for activation of the Kil system, we measured that killing is observed within ~2 min after assembly,
207 a rapid effect which suggests that NG-KilD cluster assembly is tightly connected to a prey cell
208 lytic activity (Figure S4c). We conclude that NG-KilD cluster formation spatially reports both on
209 spatial predator-prey interaction and correlate with killing.

210 We next used NG-KilD to monitor the function of the Kil Tad apparatus in prey recognition
211 and killing. In WT cells NG-KilD clusters only formed in the presence of prey cells and ~30%
212 contacts were productive for cluster formation (Figure 4d). In *kil* mutants, NG-KilD clusters still
213 formed upon prey cell contact with a minor reduction (up to ~2 fold in the *KilC* and *KilK*),
214 suggesting Tad-like apparatus is not directly responsible for initial prey cell sensing (Figure 4d,
215 Movie S6). Nevertheless cluster assembly was highly correlated to motility pauses (Figure 4e);
216 which was impaired (up to 60%) in the *kil* mutants (except in the *pilin*, *kilK* mutant) and most
217 strongly in the *kilC* (secretin), *kilG* (IM platform) and triple pilin (*kilKLM*) mutants (Figure 4e).
218 Strikingly and contrarily to WT cells, cluster formation was not followed by cell lysis in all *kil*
219 mutants, except in the major pilin *kilK* mutant (or very rarely, ~4% of the time versus more than
220 80% in WT, Figure 4f). Altogether, these results indicate the Tad-like Kil system is dispensable
221 for immediate prey recognition, but functions downstream to induce a motility pause and critically,
222 provoke prey cell lysis.

223
224 ***The Kil apparatus is central for Myxococcus predation.*** We next tested the exact contribution of
225 the *kil* genes to predation and prey consumption. This question is especially relevant because a
226 number of mechanisms have been proposed to contribute to *Myxococcus* predation and all involve
227 the extracellular secretion of toxic cargos^{9,11,12}. In pure cultures, deletion of the *kil* genes is not
228 linked to detectable motility and growth phenotypes, suggesting that the Tad-like Kil system
229 mostly operates in predatory context (Figure S4d-e). When observed by time lapse, a *kil* mutant
230 (here *kilACF*) can invade a prey colony, but no prey killing is observed (Figure 5a, Movie S7). To
231 measure the impact of this defect quantitatively, we developed a FACS-based assay that directly
232 measures the relative proportion of *Myxococcus* cells and *E. coli* cells in the prey colony across
233 time (Figure 5b, methods). In this assay, we observed that WT *Myxococcus* cells completely take
234 over the *E. coli* population after 72h (Figure 5b). In contrast, the *E. coli* population remained fully
235 viable when in contact with the a *kilACF* triple mutant, even after 72h (Figure 5b). In this assay,
236 predatory-null phenotypes were obtained in absence of selected Tad structural components,
237 secretin (*KilC*), ATPase (*KilF*) and IM platform protein (*KilH*) (Figure 5c). A partial defect was
238 observed in the pilin (*KilK*) but a triple pilin deletion mutant (*kilKLM*) was however completely
239 deficient (Figure 5c).

240 To further test whether Kil-dependent prey killing provides the necessary nutrient source
241 for prey-dependent growth, we directly imaged *Myxococcus* cell division in prey colonies, tracking
242 single cells over the course of 6 hours (Methods). This analysis revealed that invading *Myxococcus*
243 cell size increased linearly up to a certain length, which was followed by a motility pause and
244 cytokinesis (Figure 5d, Movie S8). The daughter cells immediately resumed growth at the same
245 speed (Figure 5d). Cell size and cell age are therefore linearly correlated allowing estimation of a
246 ~5.5 hours generation time from a compilation of traces (Figure 5e, n=16). When the *kilACF*
247 mutant was similarly observed, cell division was not observed and in fact cell size tended to
248 decrease with time (Figures 5d-5e, n=20). Cell shortening could be a consequence of starvation,
249 as observed for example in *Bacillus subtilis*²⁶ (although this remains to be documented in
250 *Myxococcus*). Taken together, these results demonstrate the central function of the Kil Tad
251 apparatus in prey killing and consumption.

252

253 ***The Kil system promotes killing of phylogenetically diverse prey bacteria.*** *Myxococcus* is a
254 versatile predator and can attack and digest a large number of preys^{27,28}. We therefore tested if the
255 Kil system also mediates predation by contact-dependent killing of other bacterial species. To this
256 aim, we tested evolutionarily-distant preys, diderm bacteria, *Caulobacter crescentus*, *Salmonella*
257 *typhimurium* and *Pseudomonas aeruginosa*, and monoderm, *Bacillus subtilis*. In predation plate
258 assays, *M. xanthus* was able to invade and lyse all tested preys, except *P. aeruginosa* (Figure 6a-
259 b). When the Kil system was deleted, the predation ability of *M. xanthus* was severely diminished
260 in all cases (Figure 6a-b). The importance of the Kil system was even more striking when
261 predator/prey cells were mixed together and spotted direct on a CF plate to favor immediate cell-
262 cell contacts: after 24 h, all the prey cells were killed by WT *M. xanthus*, however, almost no
263 killing was observed for the Δ *kilACF* strain (Figure S4f). Consistently, *Myxococcus* assembled
264 NG-KilD clusters in contact with *Caulobacter*, *Salmonella* and *Bacillus subtilis* cells, which in all
265 cases led to cell plasmolysis (Figure 6c-e, Movie S9-11). *Myxococcus* cells were however unable
266 to form lethal clusters when mixed with *Pseudomonas aeruginosa* cells (Movie S12), suggesting
267 that although the Kil system has a large spectrum of target species, it is not universally effective
268 and resistance/evasion mechanisms must exist.

269

270 ***The kil genes evolved in predatory bacteria.*** We next explored bacterial genomes for the presence
271 of *kil*-like genes. Phylogenetic analysis indicates that the ATPase (KilF), IM platform proteins
272 (KilH and KilG) and CpaB protein (KilB) share similar evolutionary trajectories (Supplemental
273 file 1, methods), allowing the construction of a well-supported phylogenetic tree based on a
274 supermatrix (Figure 7, Methods). This analysis reveals that Kil-like systems are indeed related to
275 Tad systems (ie Tad systems from alpha-proteobacteria, Figure 7) but they form specific clades in
276 deltaproteobacteria, specifically in *Myxococcales*, in *Bdellovibrionales* and in the recently
277 discovered *Bradymonadales*. In these bacteria, predicted Kil machineries are very similar to the
278 *Myxococcus* Kil system, suggesting a similar function (Figure 7, Table S2). Remarkably, these
279 bacteria are all predatory; the predatory cycle of *Bradymonadales* is yet poorly described but it is

280 thought to be quite similar to the *Myxococcus* predatory cycle, involving surface motility and
281 extracellular prey attack¹. At first glance, *Bdellovibrio* species use a distinct predatory process,
282 penetrating the prey cell to actively replicate in their periplasmic space². However, this cycle
283 involves a number of processes that are similar to Myxobacteria: *Bdellovibrio* cells also attack
284 prey cells using gliding motility²⁹ and attach to them using Type IV pili and a number of common
285 regulatory proteins³⁰. Prey cell penetration follows from the ability of the predatory cell to drill a
286 hole into the prey PG at the attachment site³¹. While there is currently no direct evidence that the
287 *Bdellovibrio* Kil-like system is involved in this process, multiple genetic evidence suggest that the
288 Kil homolog are important for prey invasion and attachment^{32,33}. It is therefore possible that
289 acquisition of a Tad-like system in deltaproteobacteria was key to the emergence of predation,
290 following its specialization in a possible ancestor of the *Myxococcales*, *Bdellovibrionales* and
291 *Bradymonadales*.

292

293 **Discussion.** Prior to this work, *Myxococcus* predation was thought to be multifactorial and involve
294 motility, secreted proteins, OMVs and antibiotics (ie Myxovirescin and Myxoprincomide) to kill
295 and digest preys extracellularly^{3,5}. While a contribution of these processes is not to be ruled out,
296 most likely for prey cell digestion rather than killing (for example by degradative enzymes³), we
297 show here that in association with A-motility, contact-dependent killing is the major prey killing
298 mechanism. In *Myxococcus*, contact-dependent killing can be mediated by several processes, now
299 including T6SS, OME and Kil. We exclude a function for the T6SS, for which a function in
300 *Myxococcus* interspecies interactions has yet to be demonstrated. Rather, it appears that together
301 with OME, Type VI secretion controls a phenomenon called social compatibility, in which the
302 exchange of toxins between *Myxococcus* cells prevents immune cells from mixing with non-
303 immune cells¹⁷. We have not tested a possible function of OME in prey killing because OME
304 allows transfer of OM protein and lipids between *Myxococcus* cells when contact is established
305 between identical outer membrane receptors, TraA⁹. OME is therefore highly *Myxococcus* species
306 and even strain-specific and mediates social compatibility when SitA lipoprotein toxins are
307 delivered to non-immune TraA-carrying *Myxococcus* target cells³⁴.

308 The Kil system is therefore a major component of an emerging genetic arsenal supporting
309 predation. Although we currently only assign Kil functions to the Tad apparatus, the complete Kil
310 system may be composed of numerous additional components because, in both clusters, the *tad*
311 core genes are genetically linked to a large number of conserved genes with unknown predicted
312 functions (up to 11 proteins of unknown functions just considering cluster 1 and 2, Figure 3a,
313 Table S1). This may not be surprising because contact-dependent killing is a complex process
314 involving prey recognition, motility regulation and killing. Mechanisms for each of these processes
315 remain to be discovered. The recognition mechanism is especially intriguing and mostly
316 independent from the Kil Tad system as indicated by the persistent formation of KilD clusters
317 upon contact with prey cells. KilD is essential for prey killing and its dynamics and genetic
318 dependencies suggest that it acts upstream from the Tad system, possibly signaling its assembly at
319 the prey contact site. The large number of predicted proteins with FHA²² type domains in clusters

320 1 and 2 (Table S1) suggests a function in a potential signaling cascade. In *Pseudomonas*
321 *aeruginosa*, FHA domain-proteins act downstream from a phosphorylation cascade triggered by
322 contact, allowing *Pseudomonas* to fire its T6SS upon contact³⁵. This mechanism is triggered by
323 general perturbation of the *Pseudomonas* membrane³⁶, which could also be the case for the Kil
324 system, assembly of which is provoked both by monoderm and diderm bacteria suggesting that
325 prey-specific determinants are unlikely. Recognition is nevertheless non-universal and does not
326 occur in contact with *Pseudomonas* or *Myxococcus* itself. Therefore evasion mechanisms must
327 exist, perhaps in the form of genetic determinants that shield cells from recognition.

328

329 The Kil Tad-like system itself is required for motility regulation and prey cell killing.
330 Motility regulation could be indirect because differential effects are observed depending on *kil*
331 gene deletions (Figure 3 and 4), suggesting that assembly of a functional Tad apparatus is not
332 strictly required for regulation. In contrast, prey killing requires a functional Tad apparatus. In
333 particular, the pilin proteins are required during prey invasion but they are dispensable (partially)
334 in liquid cultures where cells form clumps possibly favoring cell-cell interactions independently
335 from the Tad pilins. Thus, pilins are likely required for *Myxococcus* to latch onto prey cells but
336 they may not intervene directly in prey cell toxicity. How the pilins organize to form polymers and
337 whether they do, remains to be determined; the lack of the major pilin (KilK) is compensated by
338 the remaining pseudo-pilins KilL and M, which is somewhat surprising given that pseudopilins
339 are generally considered to prime assembly of major pilin polymers²⁰. It is currently unclear if the
340 Kil system is also a toxin-secretion device; for example, if it also functioned as a Type II secretion
341 system. Alternatively, the Kil complex might recruit a toxin delivery system at the prey contact
342 site. This latter hypothesis is in fact suggested by the remaining low (but still detectable) contact-
343 dependent toxicity of *kil* mutants (Figures 3 and 4). Given that *Myxococcus* induces prey PG
344 degradation locally, we hypothesize that a secreted cell wall hydrolase becomes active at the prey
345 contact site. This is not unprecedented: *Bdellovibrio* cells secrete a sophisticated set of PG
346 modifying enzymes, D,D-endopeptidases³⁷, L,D transpeptidases³¹ and Lysozyme-like enzymes³⁸
347 to penetrate prey cells, carve them into bdelloplasts and escape. In *Myxococcus*, deleting potential
348 D,D-endopeptidases³⁹ did not affect predation (Figure S4g) which might not be surprising given
349 that *Myxococcus* simply lyses its preys while *Bdellovibrio* needs to penetrate them while avoiding
350 their lysis to support its intracellular cycle. The *Myxococcus* toxin remains to be discovered,
351 bearing in mind, that similar to synergistic toxic T6SS effectors⁴⁰, several toxic effectors could be
352 injected, perhaps explaining how *Myxococcus* is able to kill both monoderm and diderm preys.

353

354 The discovery of the Kil system increases the functional repertoire of Type IV filament
355 nanomachines. While the Kil proteins are most similar to proteins from Tad systems, there are a
356 number of key differences that suggest profound diversification: (i), the Kil system involves a
357 single ATPase and other Tad proteins such as assembly proteins TadG, RcpB and pilotin TadD
358 are missing²⁰; (ii), several Kil proteins have unique signatures, the large number of associated
359 genes of unknown function; in particular, the over-representation of associated FHA domain

360 proteins, including the central hexameric ATPase KilF itself fused to an N-terminal FHA domain.
361 The KilC secretin is also uniquely short and lacks the N0 domain, canonically found in secretin
362 proteins⁴¹, which could be linked to increased propensity for dynamic recruitment at prey contact
363 sites. Future studies of the Kil machinery could therefore reveal how the contact-dependent
364 properties of Tad pili were adapted to prey cell interaction and intoxication, likely a key
365 evolutionary process in predatory bacteria.

366

367 **Acknowledgements**

368 We thank Lotte Søgaard-Andersen and Anke Treuner-Lange for the gift of the VipA plasmid. We
369 thank Laurent Aussel for *E. coli* plasmids, Anne Galinier for the *Bacillus subtilis* strain, Emanuele
370 Biondi for the *Caulobacter crescentus* strain and Sophie Bleves for the *Pseudomonas aeruginosa*
371 strain. We thank Dorothée Murat, Romé Voulhoux, Marcelo Nöllmann, Vladimir Pelicic and
372 Friedhelm Pfeiffer for discussions.

373 Research in TM lab was supported by a 2019 CNRS 80-Prime allowance on bacterial predation
374 and pattern formation. SS and PDB are supported by an MENRT thesis grant from the ministry of
375 research.

376

377 **Author contributions**

378 SS, JH and TM conceived the experiments and analyzed the data. SS, JH and DR performed most
379 experiments. GB ran FACS experiments and analyzed data. PDB and BH performed bioinformatic
380 analysis, homology searches, structure predictions and phylogenetic analysis. LM, EC, SS and TM
381 conceived and analyzed T6SS experiments. RM provided data with the A-S⁻ motility mutant. TM
382 wrote the paper.

383

384 **References**

385

- 386 1. Mu, D.-S. *et al.* Bradymonabacteria, a novel bacterial predator group with versatile survival
387 strategies in saline environments. *Microbiome* **8**, 126 (2020).
- 388 2. Laloux, G. Shedding Light on the Cell Biology of the Predatory Bacterium Bdellovibrio
389 bacteriovorus. *Front Microbiol* **10**, 3136 (2019).
- 390 3. Thiery, S. & Kaimer, C. The Predation Strategy of Myxococcus xanthus. *Front Microbiol* **11**, 2
391 (2020).
- 392 4. Herrou, J. & Mignot, T. Dynamic polarity control by a tunable protein oscillator in bacteria. *Curr.*
393 *Opin. Cell Biol.* **62**, 54–60 (2019).
- 394 5. Pérez, J., Moraleda-Muñoz, A., Marcos-Torres, F. J. & Muñoz-Dorado, J. Bacterial predation: 75
395 years and counting! *Environ. Microbiol.* **18**, 766–779 (2016).
- 396 6. Xiao, Y., Wei, X., Ebright, R. & Wall, D. Antibiotic production by myxobacteria plays a role in
397 predation. *J. Bacteriol.* **193**, 4626–4633 (2011).
- 398 7. Zhang, W. *et al.* Dynamics of solitary predation by Myxococcus xanthus on Escherichia coli
399 observed at the single-cell level. *Appl. Environ. Microbiol.* (2019) doi:10.1128/AEM.02286-19.
- 400 8. Troselj, V., Treuner-Lange, A., Søgaard-Andersen, L. & Wall, D. Physiological Heterogeneity
401 Triggers Sibling Conflict Mediated by the Type VI Secretion System in an Aggregative Multicellular
402 Bacterium. *mBio* **9**, (2018).

- 403 9. Sah, G. P. & Wall, D. Kin recognition and outer membrane exchange (OME) in myxobacteria.
404 *Curr Opin Microbiol* **56**, 81–88 (2020).
- 405 10. Panigrahi, S. *et al.* MiSiC, a general deep learning-based method for the high-throughput cell
406 segmentation of complex bacterial communities. *bioRxiv* 2020.10.07.328666 (2020)
407 doi:10.1101/2020.10.07.328666.
- 408 11. Mercier, R. *et al.* The polar Ras-like GTPase MglA activates type IV pilus via SgmX to enable
409 twitching motility in *Myxococcus xanthus*. *Proc Natl Acad Sci U S A* **117**, 28366–28373 (2020).
- 410 12. Islam, S. T. *et al.* Modulation of bacterial multicellularity via spatio-specific polysaccharide
411 secretion. *PLoS Biol.* **18**, e3000728 (2020).
- 412 13. Faure, L. M. *et al.* The mechanism of force transmission at bacterial focal adhesion complexes.
413 *Nature* **539**, 530–535 (2016).
- 414 14. Sun, M., Wartel, M., Cascales, E., Shaevitz, J. W. & Mignot, T. Motor-driven intracellular
415 transport powers bacterial gliding motility. *Proc. Natl. Acad. Sci. U.S.A.* **108**, 7559–7564 (2011).
- 416 15. Mignot, T., Shaevitz, J. W., Hartzell, P. L. & Zusman, D. R. Evidence that focal adhesion
417 complexes power bacterial gliding motility. *Science* **315**, 853–856 (2007).
- 418 16. Kuru, E. *et al.* In Situ probing of newly synthesized peptidoglycan in live bacteria with
419 fluorescent D-amino acids. *Angew. Chem. Int. Ed. Engl.* **51**, 12519–12523 (2012).
- 420 17. Vassallo, C. N., Troselj, V., Weltzer, M. L. & Wall, D. Rapid diversification of wild social
421 groups driven by toxin-immunity loci on mobile genetic elements. *ISME J* **14**, 2474–2487 (2020).
- 422 18. Brunet, Y. R., Espinosa, L., Harchouni, S., Mignot, T. & Cascales, E. Imaging type VI secretion-
423 mediated bacterial killing. *Cell Rep* **3**, 36–41 (2013).
- 424 19. Paradis-Bleau, C., Kritikos, G., Orlova, K., Typas, A. & Bernhardt, T. G. A Genome-Wide
425 Screen for Bacterial Envelope Biogenesis Mutants Identifies a Novel Factor Involved in Cell Wall
426 Precursor Metabolism. *PLOS Genetics* **10**, e1004056 (2014).
- 427 20. Denise, R., Abby, S. S. & Rocha, E. P. C. Diversification of the type IV filament superfamily into
428 machines for adhesion, protein secretion, DNA uptake, and motility. *PLoS Biol.* **17**, e3000390 (2019).
- 429 21. Ellison, C. K. *et al.* Obstruction of pilus retraction stimulates bacterial surface sensing. *Science*
430 **358**, 535–538 (2017).
- 431 22. Almawi, A. W., Matthews, L. A. & Guarné, A. FHA domains: Phosphopeptide binding and
432 beyond. *Prog. Biophys. Mol. Biol.* **127**, 105–110 (2017).
- 433 23. Livingstone, P. G., Millard, A. D., Swain, M. T. & Whitworth, D. E. Transcriptional changes
434 when *Myxococcus xanthus* preys on *Escherichia coli* suggest myxobacterial predators are constitutively
435 toxic but regulate their feeding. *Microb Genom* **4**, (2018).
- 436 24. Berry, J.-L. & Pelicic, V. Exceptionally widespread nanomachines composed of type IV pilins:
437 the prokaryotic Swiss Army knives. *FEMS Microbiol Rev* **39**, 1–21 (2015).
- 438 25. Friedrich, C., Bulyha, I. & Søgaard-Andersen, L. Outside-In Assembly Pathway of the Type IV
439 Pilus System in *Myxococcus xanthus*. *Journal of Bacteriology* **196**, 378–390 (2014).
- 440 26. Weart, R. B. *et al.* A metabolic sensor governing cell size in bacteria. *Cell* **130**, 335–347 (2007).
- 441 27. Morgan, A. D., MacLean, R. C., Hillesland, K. L. & Velicer, G. J. Comparative analysis of
442 myxococcus predation on soil bacteria. *Appl. Environ. Microbiol.* **76**, 6920–6927 (2010).
- 443 28. Müller, S. *et al.* Identification of Functions Affecting Predator-Prey Interactions between
444 *Myxococcus xanthus* and *Bacillus subtilis*. *J. Bacteriol.* **198**, 3335–3344 (2016).
- 445 29. Lambert, C., Fenton, A. K., Hobley, L. & Sockett, R. E. Predatory *Bdellovibrio* bacteria use
446 gliding motility to scout for prey on surfaces. *J. Bacteriol.* **193**, 3139–3141 (2011).

- 447 30. Milner, D. S. *et al.* Ras GTPase-like protein MglA, a controller of bacterial social-motility in
448 Myxobacteria, has evolved to control bacterial predation by Bdellovibrio. *PLoS Genet.* **10**, e1004253
449 (2014).
- 450 31. Kuru, E. *et al.* Fluorescent D-amino-acids reveal bi-cellular cell wall modifications important for
451 Bdellovibrio bacteriovorus predation. *Nat Microbiol* **2**, 1648–1657 (2017).
- 452 32. Avidan, O. *et al.* Identification and Characterization of Differentially-Regulated Type IVb Pilin
453 Genes Necessary for Predation in Obligate Bacterial Predators. *Sci Rep* **7**, 1013 (2017).
- 454 33. Duncan, M. C. *et al.* High-Throughput Analysis of Gene Function in the Bacterial Predator
455 Bdellovibrio bacteriovorus. *mBio* **10**, (2019).
- 456 34. Vassallo, C. N. *et al.* Infectious polymorphic toxins delivered by outer membrane exchange
457 discriminate kin in myxobacteria. *Elife* **6**, (2017).
- 458 35. Basler, M., Ho, B. T. & Mekalanos, J. J. Tit-for-tat: type VI secretion system counterattack
459 during bacterial cell-cell interactions. *Cell* **152**, 884–894 (2013).
- 460 36. Ho, B. T., Basler, M. & Mekalanos, J. J. Type 6 secretion system-mediated immunity to type 4
461 secretion system-mediated gene transfer. *Science* **342**, 250–253 (2013).
- 462 37. Lerner, T. R. *et al.* Specialized peptidoglycan hydrolases sculpt the intra-bacterial niche of
463 predatory Bdellovibrio and increase population fitness. *PLoS Pathog* **8**, e1002524 (2012).
- 464 38. Harding, C. J. *et al.* A lysozyme with altered substrate specificity facilitates prey cell exit by the
465 periplasmic predator Bdellovibrio bacteriovorus. *Nat Commun* **11**, 4817 (2020).
- 466 39. Zhang, H. *et al.* Establishing rod shape from spherical, peptidoglycan-deficient bacterial spores.
467 *Proc Natl Acad Sci U S A* **117**, 14444–14452 (2020).
- 468 40. LaCourse, K. D. *et al.* Conditional toxicity and synergy drive diversity among antibacterial
469 effectors. *Nat Microbiol* **3**, 440–446 (2018).
- 470 41. Tosi, T. *et al.* Structural similarity of secretins from type II and type III secretion systems.
471 *Structure* **22**, 1348–1355 (2014).
- 472 42. Bustamante, V. H., Martínez-Flores, I., Vlamakis, H. C. & Zusman, D. R. Analysis of the Frz
473 signal transduction system of Myxococcus xanthus shows the importance of the conserved C-terminal
474 region of the cytoplasmic chemoreceptor FrzCD in sensing signals. *Mol. Microbiol.* **53**, 1501–1513
475 (2004).
- 476 43. Shaner, N. C. *et al.* A bright monomeric green fluorescent protein derived from Branchiostoma
477 lanceolatum. *Nat. Methods* **10**, 407–409 (2013).
- 478 44. Ducret, A., Fleuchot, B., Bergam, P. & Mignot, T. Direct live imaging of cell-cell protein transfer
479 by transient outer membrane fusion in Myxococcus xanthus. *Elife* **2**, e00868 (2013).
- 480 45. Schindelin, J. *et al.* Fiji: an open-source platform for biological-image analysis. *Nat. Methods* **9**,
481 676–682 (2012).
- 482 46. Ducret, A., Quardokus, E. M. & Brun, Y. V. MicrobeJ, a tool for high throughput bacterial cell
483 detection and quantitative analysis. *Nat Microbiol* **1**, 16077 (2016).
- 484 47. Camacho, C. *et al.* BLAST+: architecture and applications. *BMC Bioinformatics* **10**, 421 (2009).
- 485 48. Altschul, S. F. *et al.* Gapped BLAST and PSI-BLAST: a new generation of protein database
486 search programs. *Nucleic Acids Res.* **25**, 3389–3402 (1997).
- 487 49. Hildebrand, A., Remmert, M., Biegert, A. & Söding, J. Fast and accurate automatic structure
488 prediction with HHpred. *Proteins* **77 Suppl 9**, 128–132 (2009).
- 489 50. Kelley, L. A., Mezulis, S., Yates, C. M., Wass, M. N. & Sternberg, M. J. E. The Phyre2 web
490 portal for protein modeling, prediction and analysis. *Nat Protoc* **10**, 845–858 (2015).

- 491 51. Waterhouse, A. *et al.* SWISS-MODEL: homology modelling of protein structures and complexes.
492 *Nucleic Acids Res.* **46**, W296–W303 (2018).
- 493 52. Pettersen, E. F. *et al.* UCSF Chimera--a visualization system for exploratory research and
494 analysis. *J Comput Chem* **25**, 1605–1612 (2004).
- 495 53. Medema, M. H., Takano, E. & Breitling, R. Detecting sequence homology at the gene cluster
496 level with MultiGeneBlast. *Mol. Biol. Evol.* **30**, 1218–1223 (2013).
- 497 54. Katoh, K., Misawa, K., Kuma, K. & Miyata, T. MAFFT: a novel method for rapid multiple
498 sequence alignment based on fast Fourier transform. *Nucleic Acids Res.* **30**, 3059–3066 (2002).
- 499 55. Guindon, S. *et al.* New algorithms and methods to estimate maximum-likelihood phylogenies:
500 assessing the performance of PhyML 3.0. *Syst. Biol.* **59**, 307–321 (2010).
- 501 56. Huson, D. H. & Scornavacca, C. Dendroscope 3: an interactive tool for rooted phylogenetic trees
502 and networks. *Syst. Biol.* **61**, 1061–1067 (2012).

503

504 **Figure Legends**

505

506 **Figure 1. A-motility is required for invasion of prey colonies.**

507 Colony plate assays showing invasion of an *E. coli* prey colony (dotted line) 48 hours after plating
508 by WT **(a)**, A⁺S⁻ **(b)** and A⁻S⁺ **(c)** strains. Scale bar = 2 mm.

509 **a1:** zoom of the invasion front. *Myxococcus* single cells are labelled with mCherry. Long arrows
510 show the movement of “arrowhead” cell groups as they invade prey colonies. Short arrows point
511 to A-motile single cells that penetrated the prey colony. Scale bar = 10 μm.

512 **a2:** zoom of invading *Myxococcus* cells the prey colony. Scale bar = 3 μm.

513 See associated Movie S1 for the full time lapse.

514 **b1:** zoom of the invasion front formed by A⁻S⁺ cells. Note that the S-motile *Myxococcus* cells come
515 in contact with the prey colony, but in absence of A-motility, the predatory cells fail to infiltrate
516 the colony and remain stuck at the border. Scale bar = 10 μm. See associated Movie S2 for the full
517 time lapse.

518

519 **Figure 2. A-motile cells kill prey cells by contact.**

520 **a:** prey (*E. coli*) colony invasion by an “arrowhead formation”. Activity of the A-motility complex
521 is followed by monitoring *Myxococcus* cells expressing the bFA-localized AglZ-YFP protein.
522 Upper panel: Cells within the arrowhead (examples shown in white) assemble bFAs (white
523 arrowheads). Lower panel: Semantic segmentation (see methods) of the total cell population, *E.*
524 *coli* (white) and *Myxococcus* (green). The colored *E. coli* cells (magenta and blue) are the ones
525 that are observed to lyse as the *Myxococcus* cells penetrate the colony. See associated Movie S3
526 for the full time lapse. Scale bar = 10 μm.

527 **b:** bFAs are disassembled when *Myxococcus* establishes lytic contacts with prey cells. Shown is
528 an AglZ-YFP expressing *Myxococcus* cell establishing contact with an mCherry-expressing *E. coli*
529 cell (overlay and phase contrast image). Note that the *Myxococcus* cell resumes movement and
530 thus re-initiates bFA formation immediately after *E. coli* cell lysis. See associated Movie S4 for
531 the full time lapse. Scale bar = 2 μm.

532 **c:** *Myxococcus* (outlined in white) provoke *E. coli* plasmolysis. Top: shown is a GFP-expressing
533 *E. coli* cell lysing in contact with a *Myxococcus* cell. GFP fluorescence remains stable for 5 min
534 after contact and becomes undetectable instantaneously, suggesting plasmolysis of the *E. coli* cell.
535 Scale bar = 2 μm . Bottom: graphic representation of fluorescence intensity loss upon prey lysis.
536 **d,e :** *Myxococcus* contact provoke local degradation of the *E. coli* peptidoglycan.
537 **d:** *E. coli* PG was labeled covalently with the fluorescent D-amino acid TADA. Two *E. coli* cells
538 lyse upon contact. Holes in the PG-labelling are observed at the contact sites (white arrows). Note
539 that evidence for plasmolysis and local IM membrane contraction is visible by phase contrast for
540 the lower *E. coli* cell (dark arrow). Scale bar = 2 μm .
541 **e:** Kymograph of TADA-labeling corresponding to the upper *E. coli* cell. At time 0 which
542 corresponds to the detection of cell lysis, a hole is detected at the contact site and propagates bi-
543 directionally from the initial site showing that the prey cell wall is degraded in time after cell death.
544 Scale bar = 1 μm .

545
546 **Figure 3. A Tad-like apparatus is required for prey recognition and contact-dependent**
547 **killing.**

548 **a:** Model structure of the Kill system following bioinformatics predictions. Annotated cluster 1
549 and cluster 2 genes are shown together with the possible localization of their protein product. Dark
550 triangles indicate the genes that were deleted in this study.

551 **b:** *kil* mutants are impaired in *E. coli* lysis in liquid. Kinetics CPRG-hydrolysis by β -Galactosidase
552 (expressed as Miller Units) observed after co-incubation of *Myxococcus* WT and *kil* mutants and
553 *E. coli* for 24 hours. *M. xanthus* and *E. coli* alone were used as negative controls. This experiment
554 was performed independently four times.

555 **c:** The percentage of contacts with *E. coli* leading to a pause in motility was calculated for *M.*
556 *xanthus* wild-type (from five independent predation movies, number of contacts n= 807) and *kil*
557 mutants (KilC: n= 1780; KilH: n= 1219; KilG: n=1141; KilB: n= 842; KilK: n=710; KilKLM: n=
558 1446)

559 **d:** the percentage of contacts with *E. coli* leading to cell lysis was also estimated.

560 In panels (b), (c) and (d), error bars represent the standard deviation of the mean. One-way
561 ANOVA statistical analysis followed by Dunnett's posttest was performed to evaluate if the
562 differences observed, relative to wild-type, were significant (*: $p \leq 0.05$, **: $p \leq 0.01$, ****:
563 $p \leq 0.0001$) or not (ns: $p > 0.05$).

564
565 **Figure 4. The Kill system assembles upon contact and causes prey cell lysis.**

566 **a,b:** NG-KillD clusters only form in contact with the prey and their formation precedes cell lysis.
567 Fluorescent micrographs and associated kymograph of the contact-induced clusters are shown.
568 Note that the clusters form at the contact site and that each prey cell lyses following cluster
569 formation. The cluster numbers in the kymograph refer to the cluster numbers in (a). Scale bar =
570 2 μm . See associated Movie S5 for the full time lapse.

571 **c:** PG-holes are formed at the cluster-assembly sites. TADA-labelled *E. coli* cells are shown in the
572 presence of NG-KilD expressing *Myxococcus xanthus* cells. PG holes and clusters are indicated
573 with white arrows. Scale bar = 2 μ m.

574 **d:** The percentage of contacts with *E. coli* leading to KilD foci formation was calculated for *M.*
575 *xanthus* wild-type (from five independent predation movies, number of contacts n= 807) and *kil*
576 mutants (KilC: n= 1780; KilH: n= 1219; KilG: n=1141; KilB: n= 842; KilK: n=710; KilKLM: n=
577 1446).

578 **e:** the percentage of KilD foci (*M. xanthus* WT: number of NG-KilD foci n= 198) and *kil* mutants
579 (KilC: n= 320; KilH: n= 270; KilG: n= 251; KilB: n= 215; KilK: n= 94; KilKLM: n= 355).
580 associated with a motility pause was also estimated.

581 **f:** the percentage of KilD foci leading to *E. coli* lysis was estimated as well.

582 In panels (d), (e) and (f), error bars represent the standard deviation to the mean. One-way ANOVA
583 statistical analysis followed by Dunnett's posttest was performed to evaluate if the differences
584 observed, relative to wild-type, were significant (*: $p \leq 0.05$, **: $p \leq 0.01$, ****: $p \leq 0.0001$) or not
585 (ns: $p > 0.05$).

586

587 **Figure 5. The *kil* genes are required for *M. xanthus* nutrition over prey cells.**

588 **a:** A *kil* mutant can invade but cannot lyse *E. coli* prey colonies. mCherry-labeled WT and triple
589 *kilACF* mutant are shown for comparison. Note that invading WT cells form corridors in the prey
590 colony and ghost *E. coli* cells as well as cell debris are left behind the infiltrating *Myxococcus*
591 cells. In contrast, while the *kilACE* penetrates the prey colony, corridors and prey ghost cells are
592 not observed. Scale bar = 10 μ m. See corresponding Movie S7 for the full time lapse.

593 **b:** the *kil* genes are essential for prey killing. *E. coli* mCherry cells were measured by FACS at
594 time 0, 24, 48 and 72 hours after the onset of predation. The *E. coli* survival index was calculated
595 by dividing the percentage of "*E. coli* events" at t=24, 48 or 72 hours by the percentage of "*E. coli*
596 events" at the beginning of the experiment (t=0). This experiment was performed over two
597 biological replicates, in total 6 samples per time point were collected. For each sample, 500,000
598 events were analyzed. Each data point indicates the mean \pm the standard deviation. For each time
599 point, unpaired t-test (with Welch's correction) statistical analysis was performed to evaluate if
600 the differences observed, relative to wild-type, were significant (***: $p \leq 0.001$) or not (ns: $p > 0.05$).

601 **c:** *E. coli* survival in the various *kil* mutant strains at 48 h. *E. coli* mCherry cells were measured
602 (counted) by FACS at time 0 and 48 h after predation. This experiment was performed over three
603 biological replicate, n= 9 per strain and time point. Events were counted as a) and each data point
604 indicates the mean \pm the standard deviation. One-way ANOVA statistical analysis followed by
605 Dunnett's posttest was performed to evaluate if the differences observed, relative to wild-type,
606 were significant (****: $p \leq 0.0001$).

607 **d, e:** The *kil* genes are essential for *Myxococcus* growth on prey.

608 **d:** cell growth during invasion. Cell is a function of cell age during invasion and can be monitored
609 over time in WT cells. In contrast, cell length tends to decrease in a *kilACF* mutant showing that
610 they are not growing. See associated Movie S8 for the full time lapse.

611 e: Quantification of cell growth in WT and *kilACF* mutant backgrounds. Each individual cell was
612 tracked for 5 hours in two biological replicates for each strain. Violin plot of the growth
613 distributions (shown as the cell size increase slopes) are shown. Statistics: Student t-test, ***:
614 $p < 0.001$.

615

616 **Figure 6: The Kill system mediates killing against diverse bacterial species.**

617 a: the *kil* genes are predation determinants against various species. To evaluate if the *M. xanthus*
618 *kil* mutant was impaired for predating on various prey, *M. xanthus* WT and Δ *kilACF* cell
619 suspensions (dashed circles) were spotted on CF agar plates next to a drop of prey cell suspension
620 and observed after 48-hour incubation. Remarkably, when predating *B. subtilis* and *S. enterica*
621 *Typhimurium*, the Δ *kilACF* mutant was observed to move on top of the prey colony surface without
622 lysing it.

623 b: quantification of the experiment shown in (a) for each species. for each picture (n=24 per
624 predator/prey couple), the lysed surface of the prey spot was measured and the percentage of the
625 total surface was determined. Error bars represent the standard deviation to the mean. Unpaired t-
626 test statistical analysis was performed to evaluate if the differences of predation observed, relative
627 to wild-type, were significant (****: $p \leq 0.0001$).

628 c: Cluster formation and subsequent contact-dependent killing of *Caulobacter crescentus*. Scale
629 bar = 2 μ m. See corresponding Movie S9 for the full time lapse.

630 b: Cluster formation and subsequent contact-dependent killing of *Salmonella enterica*
631 *Typhimurium*. Scale bar = 2 μ m. See corresponding Movie S10 for the full time lapse.

632 c: Cluster formation in contact with *B. subtilis*. See corresponding Movie S11 for the full time
633 lapse. Scale bar = 2 μ m.

634

635 **Figure 7. The Kil system is conserved in predatory delta-proteobacteria**

636 Phylogenetic tree of the Type-IV filamentous (Tff) system that gave rise to the *M. xanthus* Kil
637 system. Only the 4 well-conserved Kill system components were used for constructing the
638 phylogenetic tree. Dots indicate stable bootstrap values (> 75), classes are indicated next to species
639 names. The supermatrix alignment used to compute the tree is provided as Supplemental File 1.
640 The *M. xanthus* Kil system is also found in other *Myxococcales* and closely related systems are
641 also present *Bradymonadales* and *Bdellovibrionales*, suggesting a functional specialization related
642 to predation. The genetic organization of kil-like genes is shown for example members of each
643 orders, *Bradymonas sediminis* and *Bdellovibrio bacteriovorus* (see also table S2). The
644 nomenclature and color code for Kil homologs are the same as in Figure 3. Gene accession
645 numbers (KEGG) are shown above gene symbols.

646

647

648 **Methods**

649

650 **Bacterial strains, growth conditions, motility plates, western blotting and genetic constructs**

651 See Tables S3-S5 for strains, plasmids, and primers. *E. coli* cells were grown under standard
652 laboratory conditions in Luria-Bertani (LB) broth supplemented with antibiotics, if necessary. *M.*
653 *xanthus* strains were grown at 32°C in CYE (Casitone Yeast Extract) rich media as previously
654 described⁴². *S. enterica* Typhimurium, *B. subtilis* and *P. aeruginosa* were grown overnight at 37°C
655 in LB. *C. crescentus* strain NA1000 was grown overnight at 32°C in liquid PYE (Peptone Yeast
656 Extract). Motility plate assays were conducted as previously described⁴².

657 Western blotting was performed as previously described⁴² using a commercial polyclonal anti
658 Neon-Green antibody (Chromotek)

659 Plasmids were introduced in *M. xanthus* by electroporation. Mutants and transformants were
660 obtained by homologous recombination based on a previously reported method⁴². Clean
661 replacements and deletions were constructed by allelic exchange at the endogenous loci⁴². NG-
662 KilD was expressed in place of KilD from the original locus driven by the natural promoter.
663 Specifically, a plasmid pBJ114-NG-KilD allowing insertion in the endogenous locus was
664 constructed by fusing 650 bp upstream of the *kilD* gene with the neon-green gene⁴³ itself fused in
665 frame with the first 650 bp of the *kilD* gene. These two homology regions flank the sequence of
666 the Neon green gene that contains a 12-aa linker in the C-terminal part.

667

668 **Growth in liquid culture**

669 To compare growth rates between *M. xanthus* WT and Δ *kilACF* strains, overnight CYE cultures
670 were used to inoculate the next morning 25 ml of CYE at OD₆₀₀= 0.05. Cultures were then
671 incubated at 32°C with a shaking speed of 160 rpm. To avoid measuring cell densities at night, a
672 second set of cultures were inoculated 12 hours later. Every 4 hours, 1 ml sample of each culture
673 was used to measure optical densities at 600 nm with a spectrophotometer. The different
674 measurements were then combined into a single growth curve. This experiment was performed
675 with three independent cultures per strain.

676

677 **Predation assay on agar plates**

678 *M. xanthus* and the different prey cells (*E. coli*, *C. crescentus*, *B. subtilis*, *S. enterica* Typhimurium
679 and *P. aeruginosa*) were respectively grown overnight in 20 ml CYE and 20 ml LB at 32°C and
680 37°C. The next day, cells were pelleted and resuspended in CF medium (MOPS 10 mM pH 7.6;
681 KH₂PO₄ 1 mM; MgSO₄ 8 mM; (NH₄)₂SO₄ 0.02%; Na citrate 0.2%; Bacto Casitone 0.015%) to a
682 final Optical Density (OD₆₀₀) of 5. 10 µl of *M. xanthus* and prey cell suspensions were spotted
683 next to each other (distance between two spots: less than 1 mm) on CF 1.5% agar plates
684 supplemented or not with 0.07% glucose to allow minimal growth of the prey cells and incubated
685 at 32°C. After 48-hours incubation, pictures of the plates were taken using a Nikon Olympus SZ61
686 binocular loupe (10× magnification) equipped with a camera and an oblique filter. To measure the

687 surface percentage of the prey spot lysed by *M. xanthus*, we used ImageJ to measure the total area
688 of the spot and the lysed area.

689 To force the contact between *M. xanthus* and a prey, mixes of predator/prey were also performed
690 and spotted on CF agar plates. To do so, 200 μ l of a prey cell suspension (in CF at $OD_{600} = 5$) were
691 mixed with 25 μ l of a *M. xanthus* cell suspension (in CF, $OD_{600} = 5$) and 10 μ l of this mix were
692 spotted on CF agar plates supplemented with 0.07% glucose. As described above, pictures of the
693 plates after 24-hour incubation were taken .

694

695 **Microscope invasion predation assay and contact-dependent killing.**

696 Prey invasion was imaged by microscopy using the Bato-Hubble system (the specific details of
697 the Method are described elsewhere¹⁰). Briefly, cell suspensions concentrated to $OD_{600}=5$ were
698 spotted at 1 mm distance onto CF 1.5% agar pads and a Gene Frame (Thermo Fisher Scientific)
699 was used to sandwich the pad between the slide and the coverslip and limit evaporation of the
700 sample. Slides were incubated at 32°C for 6 hours before imaging, allowing *Myxococcus* and *E.*
701 *coli* to form microcolonies. Timelapse of the predation process was taken at 40 \times or 100 \times
702 magnification. Movies were taken at the invasion front where *Myxococcus* cells enter the *E. coli*
703 colony. To facilitate tracking, *M. xanthus* cells were labeled with fluorescence⁴⁴. Fluorescence
704 images were acquired every 30 seconds for up to 10 hours, at room temperature.

705 To image contact-dependent killing between *M. xanthus* and prey cells (*E. coli*, *C. crescentus*, *B.*
706 *subtilis*, *S. typhimurium* and *P. aeruginosa*), a simpler procedure was developed. Cells were grown
707 as described above and again resuspended in CF medium to obtain an $OD_{600}= 1$ for each strain.
708 The method differs from above, in that rather than pre-incubating and allowing *Myxococcus* and
709 prey cells to form microcolonies, the *Myxococcus* and prey cells were mixed before they were
710 spotted on a CF 1.5% agar pad to be observed under the microscope immediately. This approach
711 allowed discriminating single cell contacts more easily than during colony invasion where the cell
712 density is high. Briefly, equal volumes of *M. xanthus* and prey cell suspensions were mixed
713 together and 1 μ l was spotted on a freshly made CF 1.5% agar pad on a microspore slide. After
714 the spot has dried, the agar pad was covered with a glass coverslip, and the slide was left in the
715 dark at room temperature for 20-30 minutes before imaging.

716

717 **Labelling *E. coli* cells with the fluorescent D-Amino Acid TADA**

718 Lyophilized TADA (MW = 381.2g/mol, laboratory stock¹³) was re-suspended in DMSO at 150
719 mM and conserved at -20°C. The labeling was performed, for 2 h in the dark at room temperature,
720 using 2 μ l of the TADA solution for 1ml of cells culture ($OD_{600} = 2$). Cells were then washed four
721 times with 1ml of CF and used directly for predation assays on agar pad.

722

723 **Epifluorescence Microscopy**

724 Time-lapse experiments were performed using two automated and inverted epifluorescence
725 microscope: a TE2000- E-PFS (Nikon), with a $\times 100/1.4$ DLL objective and an ORCA Flash 4.0LT
726 camera (Hamamatsu) or a Ti Nikon microscope equipped with an ORCA Flash 4.0LT camera
727 (Hamamatsu). These microscopes are equipped with the “Perfect Focus System” (PFS) that
728 automatically maintains focus so that the point of interest within a specimen is always kept in sharp
729 focus at all times, despite any mechanical or thermal perturbations. Images were recorded with
730 NIS software from Nikon. All fluorescence images were acquired with appropriate filters with a
731 minimal exposure time to minimize photo-bleaching and phototoxicity effects: 30-minute long
732 time lapses (one image acquired every 30 seconds) of the predation process were taken at 100X
733 magnification. DIA images were acquired using a 5 ms light exposure and GFP fluorescent images
734 were acquired using a 100 ms fluorescence exposure with power intensity set to 50% (excitation
735 wavelength 470 nm) to avoid phototoxicity

736 **Image Analysis**

737 Image analysis was performed under FIJI⁴⁵ and MicrobeJ⁴⁶ an ImageJ plug-in for the analysis of
738 bacterial cells.

739 Semantic segmentation of *Myxococcus* cells was obtained using the newly developed MiSiC
740 system, a deep learning based bacterial cell segmentation tool¹⁰. The system was used in semantic
741 segmentation mode and annotated manually to reveal *E. coli* lysing cells.

742 Kymographs construction: Kymographs were obtained after manual measurements of
743 fluorescence intensities along FIJI hand-drawn segments and the FIJI-Plot profile tool. The
744 measurements were then exported into the Prism software (Graphpad, Prism 8) to construct
745 kymographs.

746 Cell tracking: Cell tracking and associated morphometrics were obtained using MicrobeJ. Image
747 stacks were first processed stabilized and filtered with a moderate Gaussian blur and cells were
748 detected by thresholding and fitted with the Plug-in “medial axis” model. Trajectories were
749 systematically verified and corrected by hand when necessary.

750 Tracking *Myxococcus* pauses in contact with preys, NG-KilD foci formation and prey cell lysis:
751 in 30-minute time lapses, contacts between prey cells and *Myxococcus* cells were scored. Pauses
752 were counted when the predatory cell stopped all movement upon contact with the prey. We also
753 counted if these contacts lead to the formation of NG-KilD foci and to cell lysis. Thus, for a
754 determined *E. coli* cell, we scored the number of contacts with *Myxococcus*, the number of pauses
755 these contacts induces in *M. xanthus* motility, the number of NG-KilD foci formed upon contacts
756 and, ultimately, the lysis of the cell. Five independent movies were analyzed for each strain and
757 the percentage of contacts leading to a pause in motility, NG-KilD foci formation and cell lysis
758 was calculated. We also estimated the percentage of NG-KilD clusters leading to cell lysis

759 Tracking cluster time to lysis: Time to lysis measures the elapsed time between cluster appearance
760 to prey cell death. Data were obtained from two biological replicates.

761

762 **CPRG assay for contact-dependent killing in liquid.**

763 As previously described, cells were grown overnight, pelleted and resuspended in CF at OD₆₀₀ ~5.
764 100 µl of *M. xanthus* cell suspension (WT and mutants) were mixed with 100 µl of *E. coli* cell
765 suspension in a 24-well plate containing, in each well, 2 ml of CF medium supplemented with
766 CPRG (Sigma aldrich, 20 µg/ml) and IPTG (Euromedex, 50 µM) to induce *lacZ* expression. The
767 plates were then incubated at 32°C with shaking and pictures were taken after 24 and 48 hours of
768 incubation. To test the contact-dependance, a two-chamber assay was carried out in a Corning 24
769 well-plates containing a 0.4-µm pore polycarbonate membrane insert (Corning Transwell 3413).
770 This membrane is permeable to small metabolites and proteins and impermeable to cells. *E. coli*
771 cells were inoculated into the top chamber and *M. xanthus* cells into the bottom chamber.

772 To evaluate the predation efficiency of the different *kil* mutants, the CPRG assay was adapted as
773 follow: wild-type DZ2 and the *kil* mutant strains were grown overnight in 15 ml of CYE. *E. coli*
774 was grown overnight in 15 ml of LB. The next morning, *M. xanthus* and *E. coli* cells were pelleted
775 and resuspended in CF at OD₆₀₀ = 0.5 and 10, respectively. To induce expression of the β-
776 galactosidase, IPTG (100 µM final) was added to the *E. coli* cell suspension.

777 In a 96-well plate, 100 µl of *M. xanthus* cell suspension were mixed with 100 µl of *E. coli* cell
778 suspension. Wells containing only *M. xanthus*, *E. coli* or CF were used as controls. The lid of the
779 96-well plate was then sealed with a breathable tape (Greiner bio-one) and the plate was incubated
780 for 24 hours at 32°C while shaking at 220 rpm. The next day, the plate was centrifuged 10 minutes
781 at 4800 rpm and 25 µl of the supernatant were transferred in a new 96-well plate containing 125
782 µl of Z-buffer (Na₂HPO₄ 60 mM, NaH₂PO₄ 40 mM, KCl 10 mM pH7) supplemented with 20
783 µg/ml of CPRG. After 15-30 minutes of incubation at 37°C, the enzymatic reaction was stopped
784 with 65 µl of Na₂CO₃ (1 M) and the absorbance at 576 nm was measured using a TECAN Spark
785 plate reader.

786 This experiment was performed independently four times. For Miller unit calculation, after CF
787 absorbance of the blank (with CF) reaction was subtracted, the absorbances measured at 576 nm
788 were divided by the incubation time and the volume of cell lysate used for reaction. The resulting
789 number was then multiplied by 1000.

790

791

792 **Fluorescence-Activated Cell Sorting (FACS) measurements of *E. coli* killing**

793 *M. xanthus* strains (wild-type and *Kil* system mutants) constitutively expressing GFP were grown
794 overnight in liquid CYE without antibiotics. *E. coli* mCherry (prey) was grown overnight in liquid

795 LB supplemented with ampicillin (100 µg/ml). The next morning, optical densities of the cultures
796 were adjusted in CF medium to OD₆₀₀= 5. *M. xanthus* GFP and *E. coli* mCherry cell suspensions
797 were then spotted onto fresh CF 1.5% agar plates as previously described⁴². Briefly, 10-µl drops
798 of the prey and the predator cell suspensions were placed next to each other and let dry. Inoculated
799 plates were then incubated at 32°C. Time 0 corresponds to the time at which the prey and the
800 predator spots were set on the CF agar plate. At time 0, 24, 48 and 72 hours (post predation) and
801 for each *M. xanthus* strain, two predator/prey spot couples were harvested with a loop and
802 resuspended in 750 µl of TPM. To fix the samples, paraformaldehyde (32% in distilled water,
803 Electron Microscopy Sciences) was then added to the samples to a final concentration of 4%. After
804 10-min incubation at room temperature, samples were centrifuged (8 min, 7500 rpm), cell pellets
805 were then resuspended in fresh TPM and optical densities were adjusted to OD₆₀₀ ~0.1.
806 Samples were then analyzed by flow cytometry. Flow cytometry data were acquired on a Bio-Rad
807 S3e Cell Sorter and analyzed using the ProSort software, version 1.6. For each sample, a total
808 population of 500,000 events was used and events corresponding to the sum of *M. xanthus*-GFP
809 and *E. coli*-mCherry. A blue laser (488 nm, 100mW) was used for detection of forward scatter
810 (FSC) and side scatter (SSC) and for excitation of GFP. A yellow-green laser (561 nm, 100 mW)
811 was used for excitation of mCherry. GFP and mCherry signals were collected using, respectively,
812 the emission filters FL1 (525/30 nm) and FL3 (615/25 nm) and a compensation was applied on the
813 mCherry signal. Samples were run using the low-pressure mode (10,000 particles/s). To calibrate
814 the instrument and reduce background noise, suspensions of fluorescent and non-fluorescent *M.*
815 *xanthus* and *E. coli* cells were used: a threshold was applied on the FSC signal, and voltages of the
816 photomultipliers for FSC, SSC, FL1 and FL3 were also adjusted. The density plots obtained (small
817 angle scattering FSC versus wide angle scattering SSC signal) were first gated on the overlapped
818 population of *M. xanthus* and *E. coli*, filtered to remove the multiple events and finally gated for
819 high FL1 signal (*M. xanthus*-GFP) and high FL3 signal (*E. coli*-mCherry).

820

821 **Bioinformatic analyses**

822 **Homology search strategy**

823 We used several search strategies to identify all potential homologous proteins of the Kil system:
824 we first used BLAST^{47,48} to search for reciprocal best hits (RBH) between the *M. xanthus* and the
825 *B. bacteriovorus* and *B. Sediminis* Kil systems, as well as the *C. crescentus* Tad system, identifying
826 *bona fide* orthologs between the three species. We limited the search space to the respective
827 proteomes of the three species. We then used HHPRED⁴⁹ to search for remotely conserved
828 homologs in *B. bacteriovorus* using the proteins from the two operons identified in *M. xanthus*.
829 Finally, we performed domain comparisons between proteins from the *B. bacteriovorus* and *B.*
830 *sediminis* Kil operons and *C. crescentus* Tad system to identify proteins with similar domain
831 compositions in *M. xanthus*. Identified orthologs or homologs between the three species, the
832 employed search strategy, as well as resulting e-values are shown in Table S2. HHPRED
833 alignments are shown in Supplemental File 1.

834

835 **Structure predictions**

836 Tertiary structural models of secretin and cytoplasmic ATPase were done using Phyre2⁵⁰ or
837 SWISS-MODEL⁵¹, in both cases using default parameters. Quaternary models were generated
838 using SWISS-MODEL. Structural models were displayed using Chimera⁵² and further processed
839 in Illustrator™.

840

841 **Phylogenetic analyses**

842 We used the four well-conserved Kill system components for phylogenetic analysis. To collect
843 species with secretion systems similar to the Kill system, we first used MultiGeneBLAST⁵³ with
844 default parameters. Orthologs of the four proteins from *B. bacteriovorus*, *B. Sediminis* and *C.*
845 *crescentus* from closely related species were added manually. We aligned each of the four proteins
846 separately using MAFFT⁵⁴ and created a supermatrix from the four individual alignments.
847 Gblocks⁵⁴ using relaxed parameters was used prior to tree reconstruction to remove badly aligned
848 or extended gap regions. The resulting alignment is shown in Suppl. File 1. Alignments of
849 individual trees were also trimmed using Gblocks. PhyML⁵⁵ was used for tree reconstruction, using
850 the JTT model and 100 bootstrap iterations. Trees were displayed with Dendroscope⁵⁶ and further
851 processed in Illustrator™.

852

853

854 **Extended Figure Legends**

855

856 **Figure S1. The motility complexes and the Type-6 Secretion System do not mediate contact-** 857 **dependent killing.**

858 **a:** Contact-dependent killing by an A⁻S⁻ motility mutant (*aglQ pilA*). Growth of *E. coli* cells leads
859 to contact with non-motile *Myxococcus* cells and rapid lysis. Example cell reflects events observed
860 for n=20 events. Scale bar = 2 μm.

861 **b:** Contact-dependent killing by a $\Delta t6ss$ motility mutant. *E. coli* prey cells are labeled with GFP
862 to monitor contact-dependent lysis. Example cell reflects events observed for n=20 events. Scale
863 bar = 2 μm.

864 **c-d:** T6SS VipA sheath assembly in *Myxococcus* cells during predation. Several assembly patterns
865 are observed as described in other bacteria. Stretched: extended T6SS sheaths. Contracted:
866 retracted T6SS sheath. Scale bars = 2 μm.

867 **e:** Prey contact-dependent lysis is not correlated to T6SS sheath contraction. Contact-dependent
868 lysis and VipA-GFP dynamics were observed simultaneously. Contraction and lysis at the
869 contacted site were only marginally observed (correlated) suggesting that T6SS intoxication plays
870 a minor role at best in contact-dependent killing.

871

872 **Figure S2. Contact-dependent lysis in liquid cultures.**

873 *E. coli* lysis is detected as extracellular release of LacZ allows hydrolysis of CPRG which becomes
874 colored. Lysis is not observed when *Myxococcus* and *E. coli* are separated by a membrane, showing
875 that it is contact-dependent.

876

877 **Figure S3: Bioinformatics analyses of Kil proteins.**

878 **a, b:** Structural models of the putative KilC secretin (a) and KilF hexameric ATPase (b). KilC
879 Secretin: tertiary and quaternary structural models were based on the structure of *Escherichia coli*
880 type II secretion system GspD protein D (PDB identifier 5WQ7) and generated with SWISS-
881 MODEL (Methods). ATPase: modeled with Phyre2 and SWISS-MODEL based on the structure
882 of the *Sulfolobus acidocaldarius* FlaI ATPase (PDB identifier 4II7).

883 **c,d:** Analysis of putative pseudo-pilin proteins. For clarity, the multiple alignment is separated in
884 three blocks representing the three different groups, the alpha-proteobacteria, the *Myxococcales*
885 and the *Bdellovibrionales*. All sequences except the one from *C. fuscus* were taken from HHPRED
886 matrix alignments. Residues conserved between the pfam domains TadF and the MXAN_4660
887 family, as well as TadE and the MXAN_4658 family, respectively, are highlighted in cyan; those
888 conserved between the Bd0115 family and the MXAN_4660 family, as well as TadE and the
889 MXAN_4658 family, respectively are highlighted in brown; residues conserved in all (TadF,
890 MXAN_4660, Bd0115, TadE, MXAN_4658, Bd0115, respectively) are highlighted in red.

891 **c:** HHPRED-based multiple sequence alignment of MXAN_4660 (KilM) with the TadF domain
892 and pilus assembly protein Bd0115 from *B. bacteriovorus*. Myxobacterial sequences correspond
893 to the following NCBI RefSeq IDs: *Myxococcus xanthus*: WP_011554652; *Myxococcus stipitatus*:
894 WP_015350653; *Myxococcus macrosporus*: WP_043711698; *Stigmatella aurantiaca*:
895 WP_013376800; *Cystobacter fuscus*: WP_002624349.

896 **d:** HHPRED-based multiple sequence alignment of MXAN_4658 with the TadE domain and pilus
897 assembly protein Bd0115 from *B. bacteriovorus*. Myxobacterial sequences correspond to the
898 following NCBI RefSeq IDs: *M. xanthus*: WP_011554650; *M. stipitatus*: WP_015350651; *M.*
899 *macrosporus*: WP_043711696; *S. aurantiaca*: WP_013376798; *C. fuscus*: WP_002624796.

900

901 **Figure S4: Functional analysis of *kil* genes.**

902 **a:** The *kil* genes are expressed during starvation. RNA-seq analysis of *kil* gene expression in rich
903 medium, starvation medium and starvation medium with live prey cells extracted and computed
904 from data by Livingstone et al.²³. For each gene and condition the data is compiled from three
905 independent biological replicates²³. Note addition of prey does not change the expression profile
906 which is significantly induced by starvation alone.

907 **b:** Stable expression of NG-KilD in mutant backgrounds. NG-KilD is detected at the expected
908 molecular weight by the anti-neonGreen antibody. -NG: DZ2 *Myxococcus* cell extracts that do not
909 express neonGreen. Dotted line indicates gel splicing.

910 **c:** Time to lysis after cluster formation. Time to lysis was determined by first monitoring cluster
911 formation and then loss of contrast by the prey cell. The measurements were performed over two
912 biological replicates. The median is shown as a red bar.

913 **d:** Growth and motility of WT and *kilACF* mutant strains on agar supporting both A- and S-motility
914 (1.5%) and S-motility only (0.5%). Scale bar = 2 mm.

915 **e:** Growth curves of WT and *kilACF* mutant in CYE rich medium. The measurements were
916 performed over three biological replicates.

917 **f:** the *kil* genes are essential for contact-dependent killing of various species in a strain mix assay.
918 To evaluate if *M. xanthus kil* mutant has lost the ability to lyse by direct contact different preys,
919 prey-cell suspensions were directly mixed with *M. xanthus* WT or Δ *kilACF* and spotted on CF agar
920 (+ 0.07% glucose). After 24-hour incubation, pictures of the spots corresponding to the different
921 predator/prey couples were taken. Note that *Pseudomonas aeruginosa* is also resistant in this assay.

922 **g:** Predation phenotype of a *Myxococcus* D,D-decarboxylase mutant³⁹. Colony plate assays
923 showing invasion of an *E. coli* prey colony (dotted line) 48 hours after plating by a *dacB* mutant.
924 Scale bar = 2 mm.

925

926

927 **Legends to Supplemental Movies**

928

929 **Movie S1: Invasion of *E. coli* colonies by WT *Myxococcus* cells.** This movie was taken at the
930 interface between the two colonies during invasion. The movie is a 8x compression of an original
931 movie that was shot for 10 hours with a frame taken every 30s at 40× magnification. To facilitate
932 *Myxococcus* cells tracking, the A⁻S⁺ (*ΔaglQ*) strain was labeled with the mCherry fluorescent
933 protein.

934

935 **Movie S2: A-motility is required for prey invasion.** This movie was taken at the interface
936 between the two colonies during invasion. The movie is a compression of an original movie that
937 was shot for 10 hours with a frame taken every 30s at 40× magnification. To facilitate *Myxococcus*
938 cells tracking, the A⁻S⁺ (*ΔaglQ*) strain was labeled with the mCherry fluorescent protein.

939

940 **Movie S3: Prey invasion by A-motile cells in “arrowhead” formations.** Focal adhesions and
941 thus active A-motility complexes were detected with an AglZ-Neon green fusion. The movie
942 contains 51 frames taken every 30 seconds at 100× magnification. Shown side-by-side are
943 fluorescence images, fluorescence overlaid with phase contrast and MiSiC segmentation (lysing
944 *E. coli* cells are colored magenta and blue).

945

946 **Movie S4: A *Myxococcus* cell kills an *E. coli* cell by contact.** The *Myxococcus* cell expresses
947 AglZ-nG and the *E. coli* cell expresses mCherry. Shown side-by-side are fluorescence images and
948 MiSiC segmentation (*Myxococcus*: green, *E. coli*: magenta). The movie contains 20 frames taken
949 every 30 seconds at 100× magnification.

950

951 **Movie S5: NG-KilD cluster formation in contact with *E. coli* prey cells.** Shown is an overlay
952 of the fluorescence and phase contrast images of a motile *Myxococcus* cell in predatory contact

953 with three *E. coli* cells. The movie was shot at 100× magnification objective for 15 minutes.
954 Pictures were taken every 30 seconds.

955

956 **Movie S6: KiID clusters form in a *kilC* mutant but cell pauses and prey killing is not observed.**

957 Shown is an overlay of the fluorescence and phase contrast images of a motile *Myxococcus* cell in
958 predatory contact with three *E. coli* cells. The movie was shot at 100× magnification objective for
959 15 minutes. Pictures were taken every 30 seconds.

960

961 **Movie S7: a *kilACF* still invades but does not kill *E. coli* prey cells.** This movie was taken at
962 the interface between the two colonies during invasion. The movie is a 4x compression of an
963 original movie that was shot for 4.5 hours with a frame taken every 30s at 40× magnification. To
964 facilitate *Myxococcus kilACF* cells are labeled with the mCherry fluorescent protein.

965

966 **Movie S8: Predatory cells division and tracking during invasion of prey colony.** To follow
967 cell growth and division at the single cell level during prey invasion, WT cells were mixed with a
968 WT strain expressing the mCherry at a 50:1 ratio and imaged every 30 seconds at 40×
969 magnification for up to 10 hours within non-labeled prey colonies. Cell growth was measured by
970 fitting cell contours to medial axis model followed by tracking under Microbe-J. Real time of the
971 track for the example cell: 95 min.

972

973 **Movie S9: NG-KiID cluster formation in contact with *Caulobacter crescentus* prey cells.**

974 Shown is an overlay of the fluorescence and phase contrast images of a motile *Myxococcus* cell in
975 predatory contact with a *C. crescentus* cell. The movie was shot at 100× magnification objective
976 for 30 minutes. Pictures were taken every 30 seconds.

977

978 **Movie S10: NG-KiID cluster formation in contact with *Salmonella typhimurium* prey cells.**

979 Shown is an overlay of the fluorescence and phase contrast images of a motile *Myxococcus* cell in
980 predatory contact with an *S. enterica* Typhimurium cell. The movie was shot at 100× magnification
981 objective for 15 minutes. Pictures were taken every 30 seconds.

982

983 **Movie S11: NG-KiID cluster formation in contact with *Bacillus subtilis* prey cells.** Shown is
984 an overlay of the fluorescence and phase contrast images of a motile *Myxococcus* cell in predatory
985 contact with a *B. subtilis* cell. The movie was shot at 100× magnification objective for 30 minutes.
986 Pictures were taken every 30 seconds.

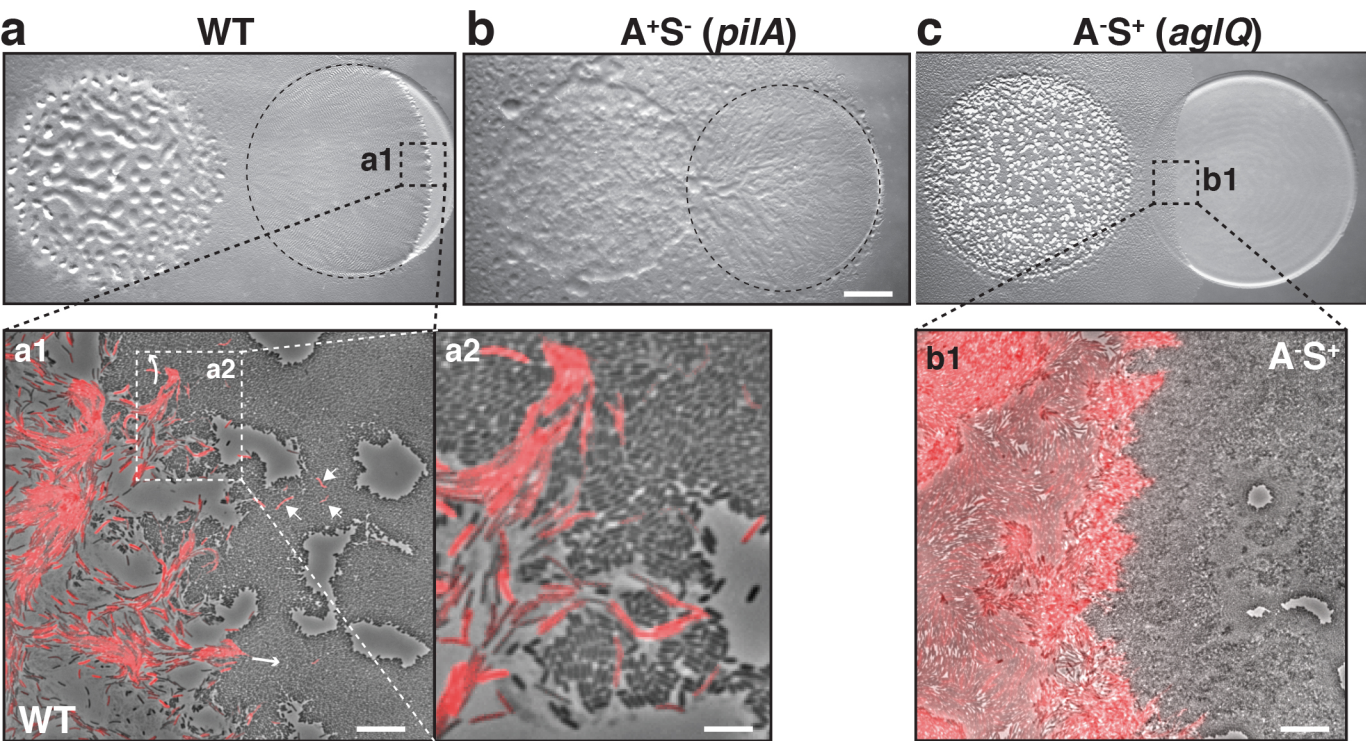
987

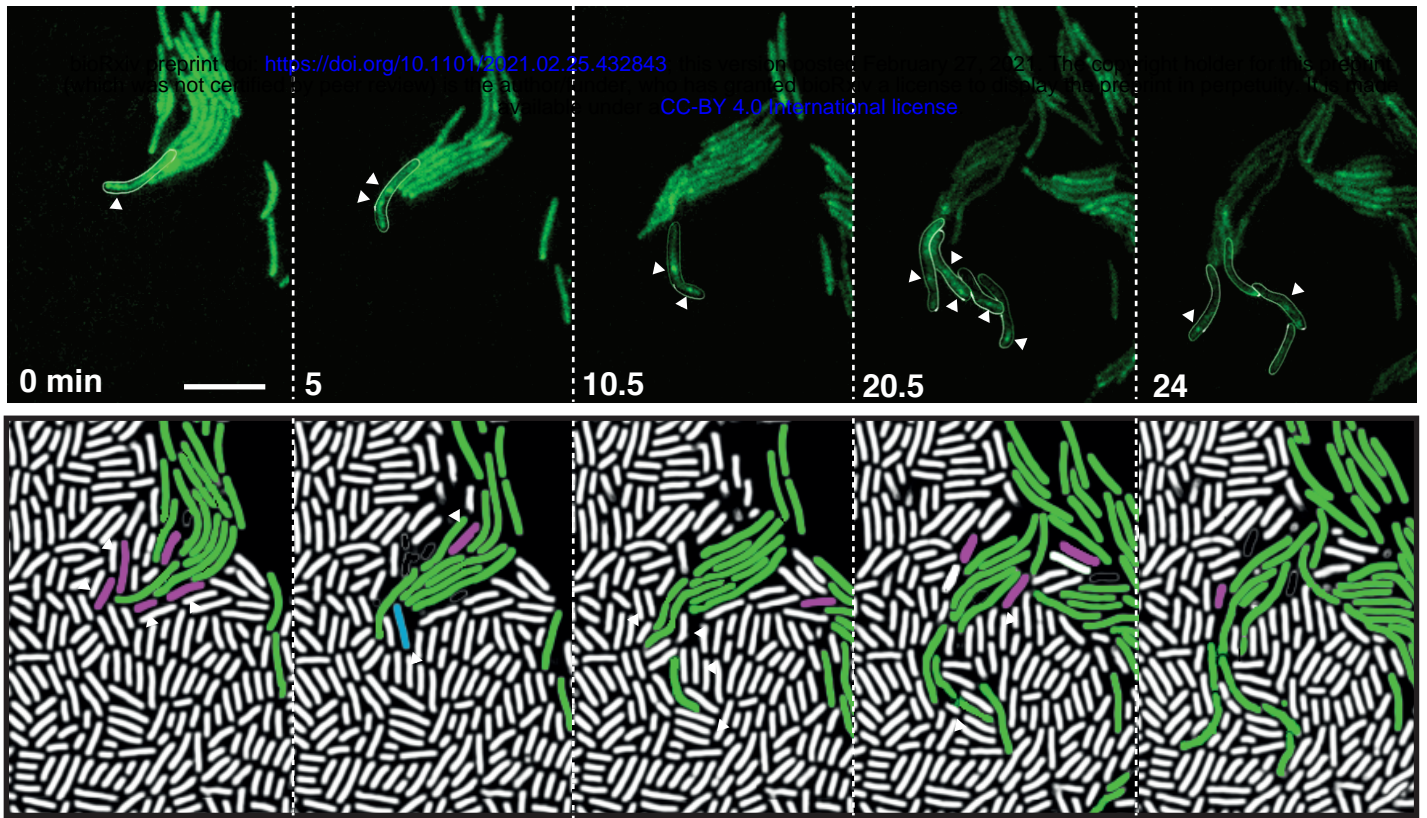
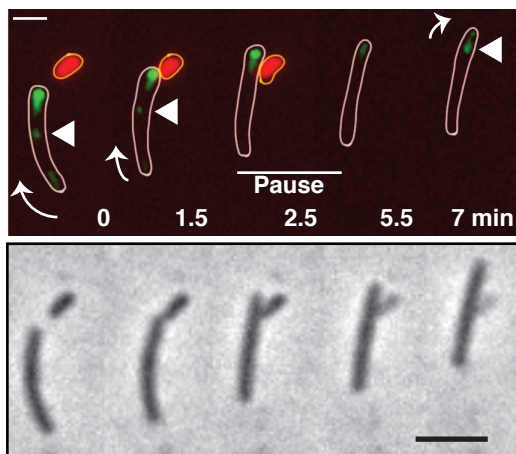
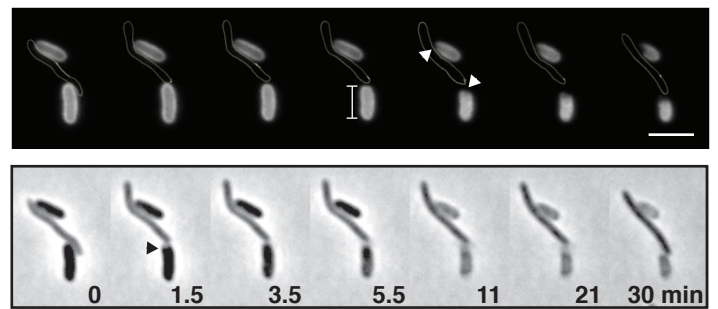
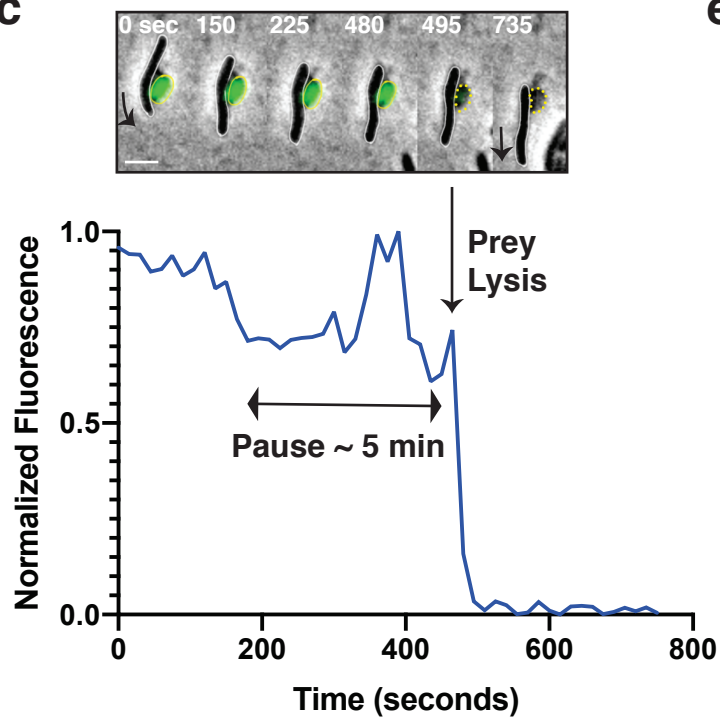
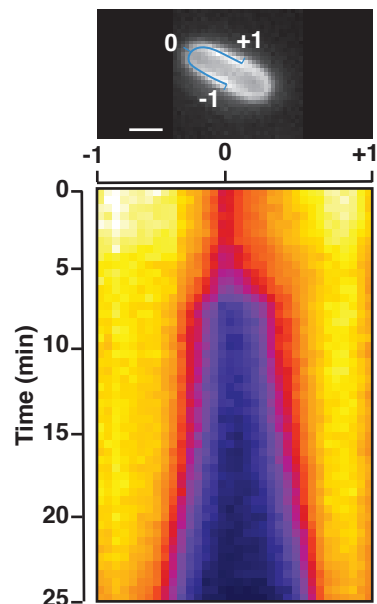
988 **Movie S12: *Pseudomonas aeruginosa* is not lysed by *Myxococcus* and does not induce NG-
989 KiID cluster formation.** Shown is an overlay of the fluorescence and phase contrast images of a
990 motile *Myxococcus* cells mixed with *Pseudomonas* cells. The movie was shot at 100×
991 magnification objective for 30 minutes. Pictures were taken every 30 seconds.

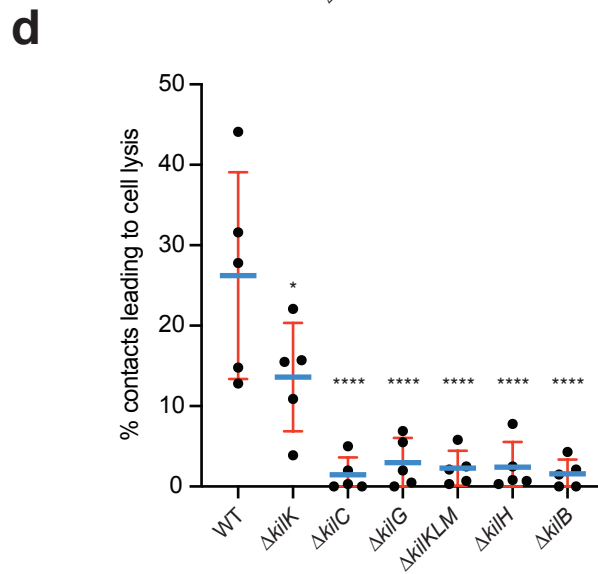
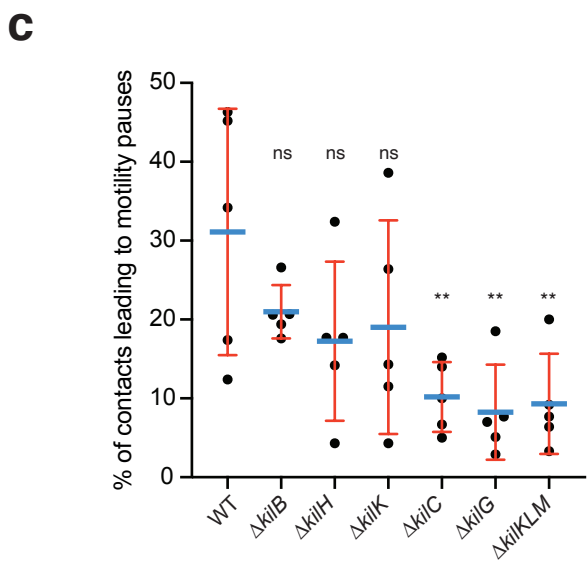
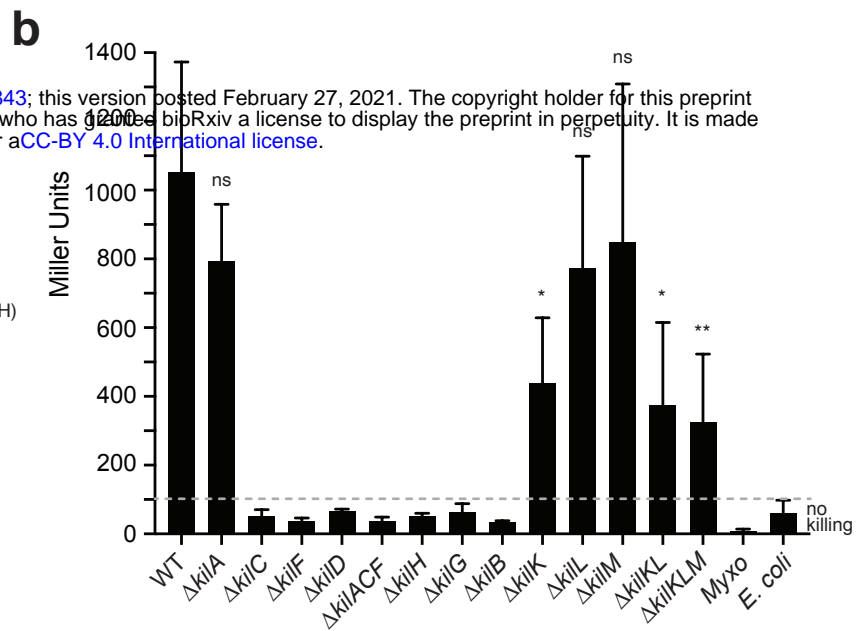
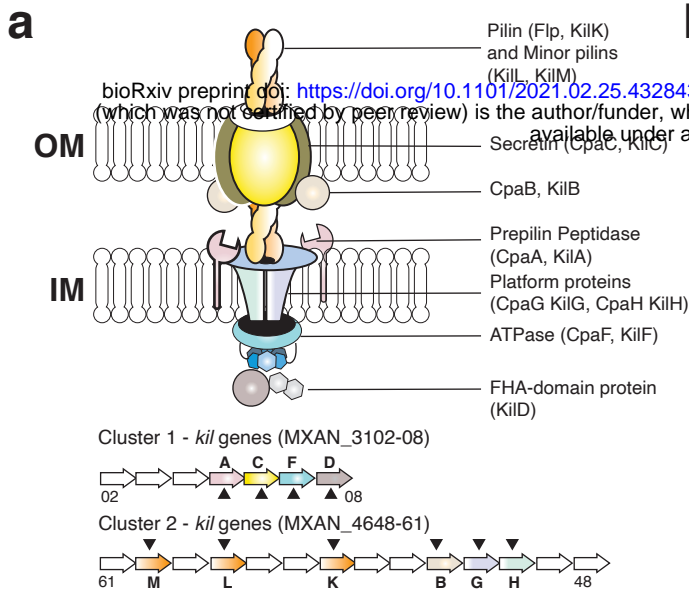
992

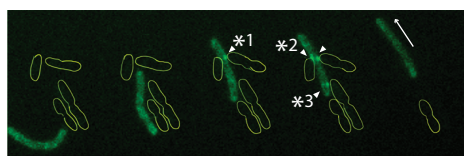
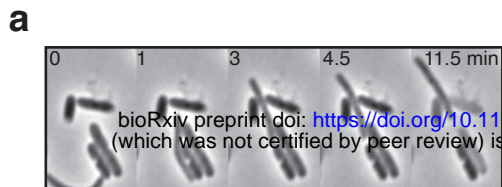
993

994

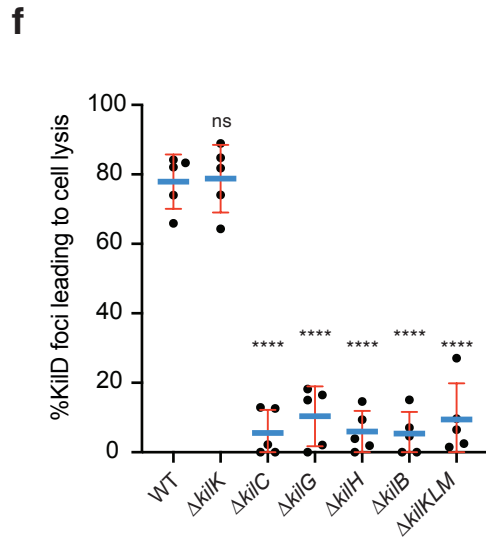
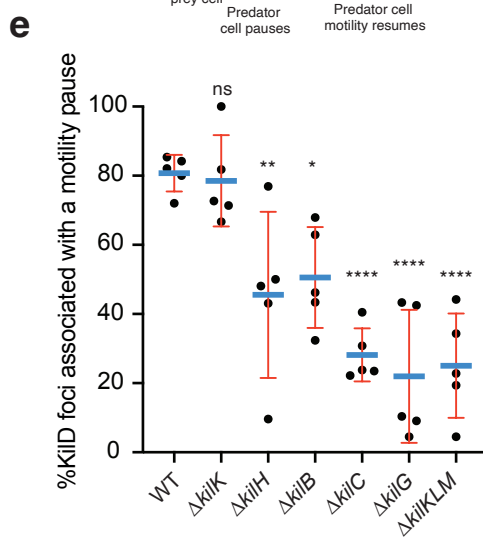
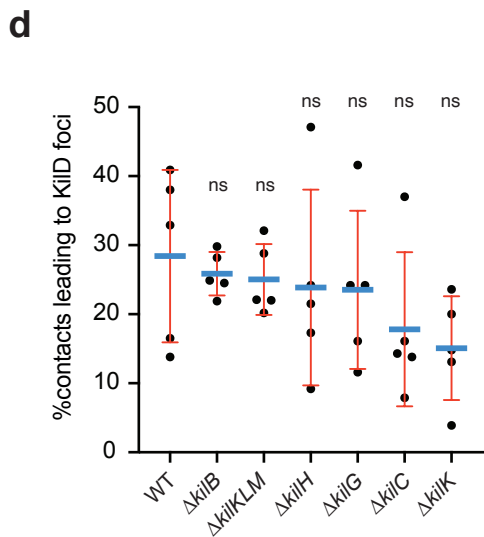
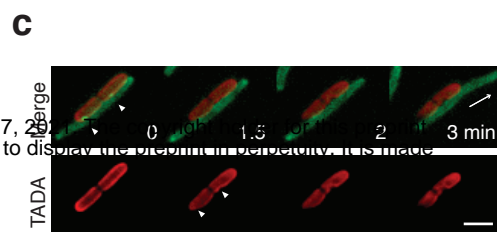
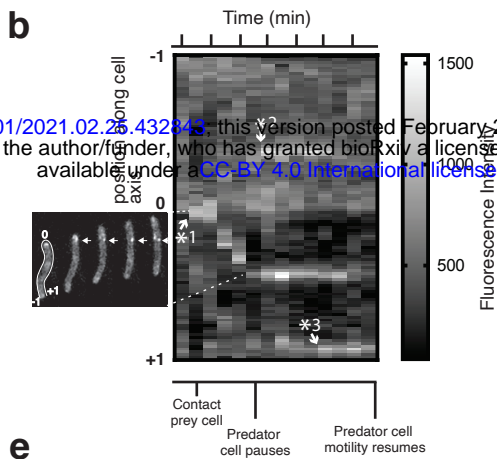


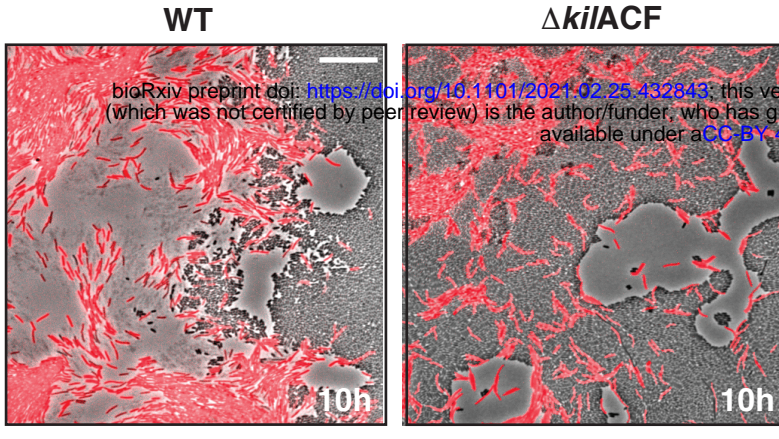
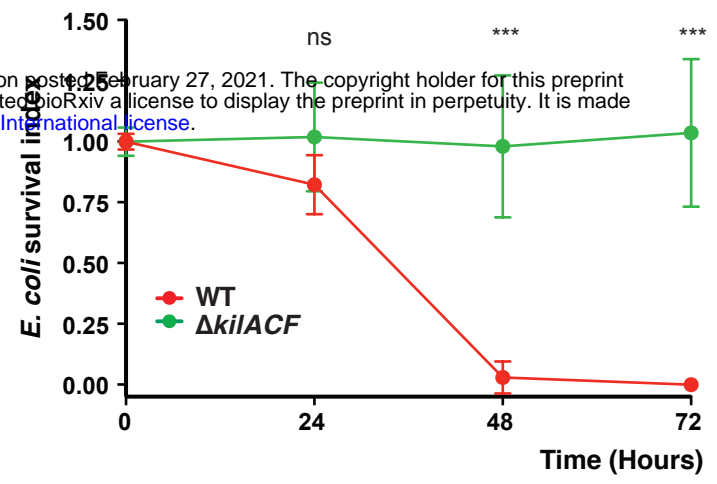
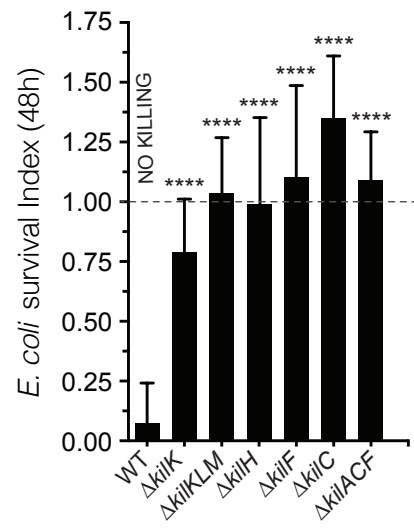
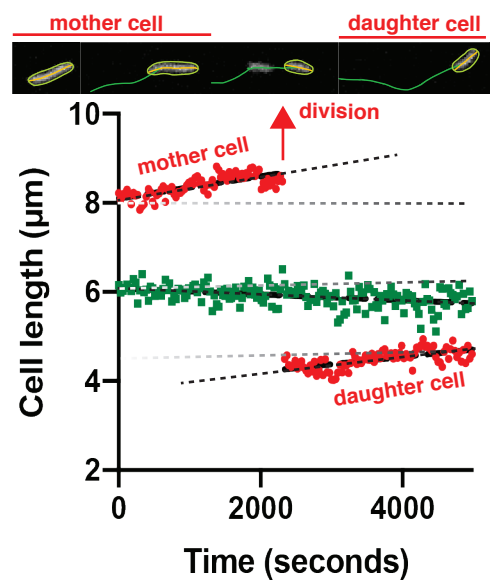
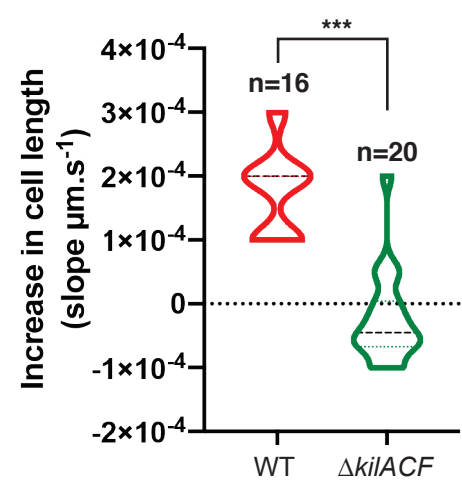
a**b****d****c****e**

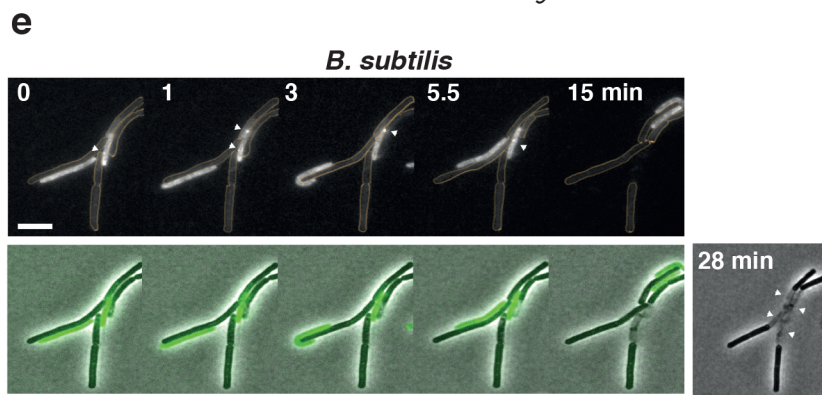
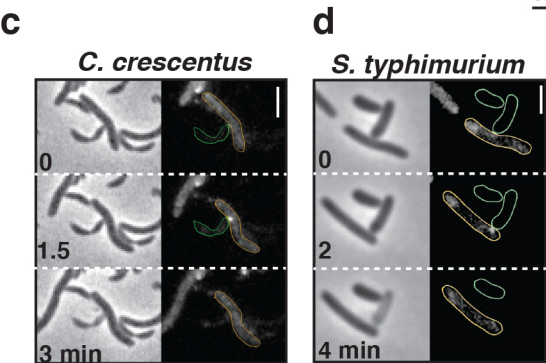
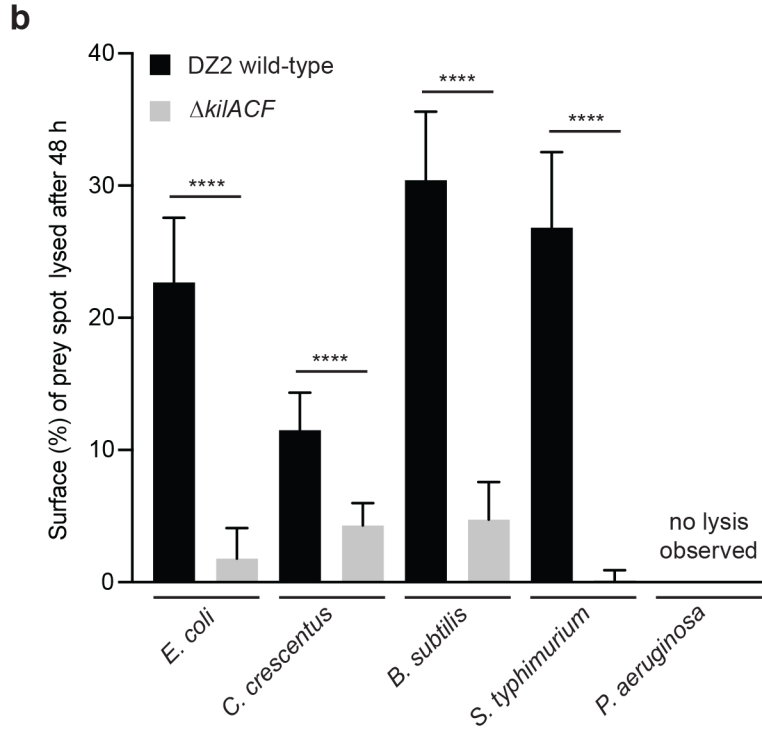
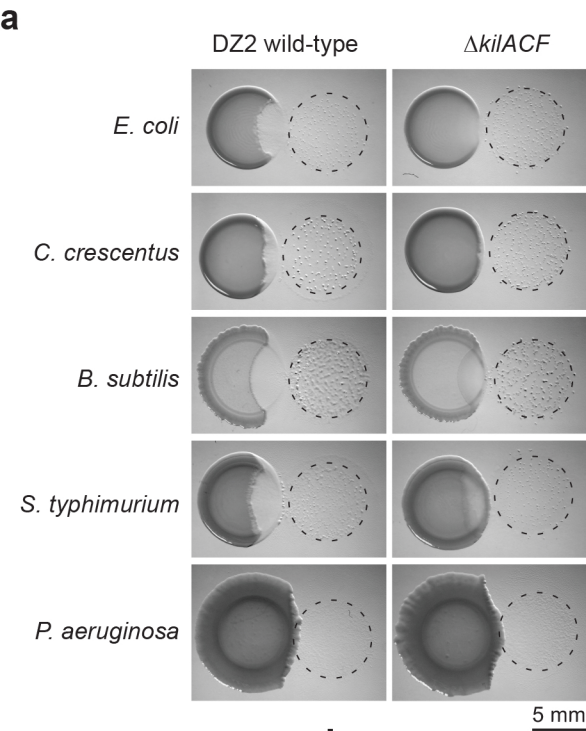


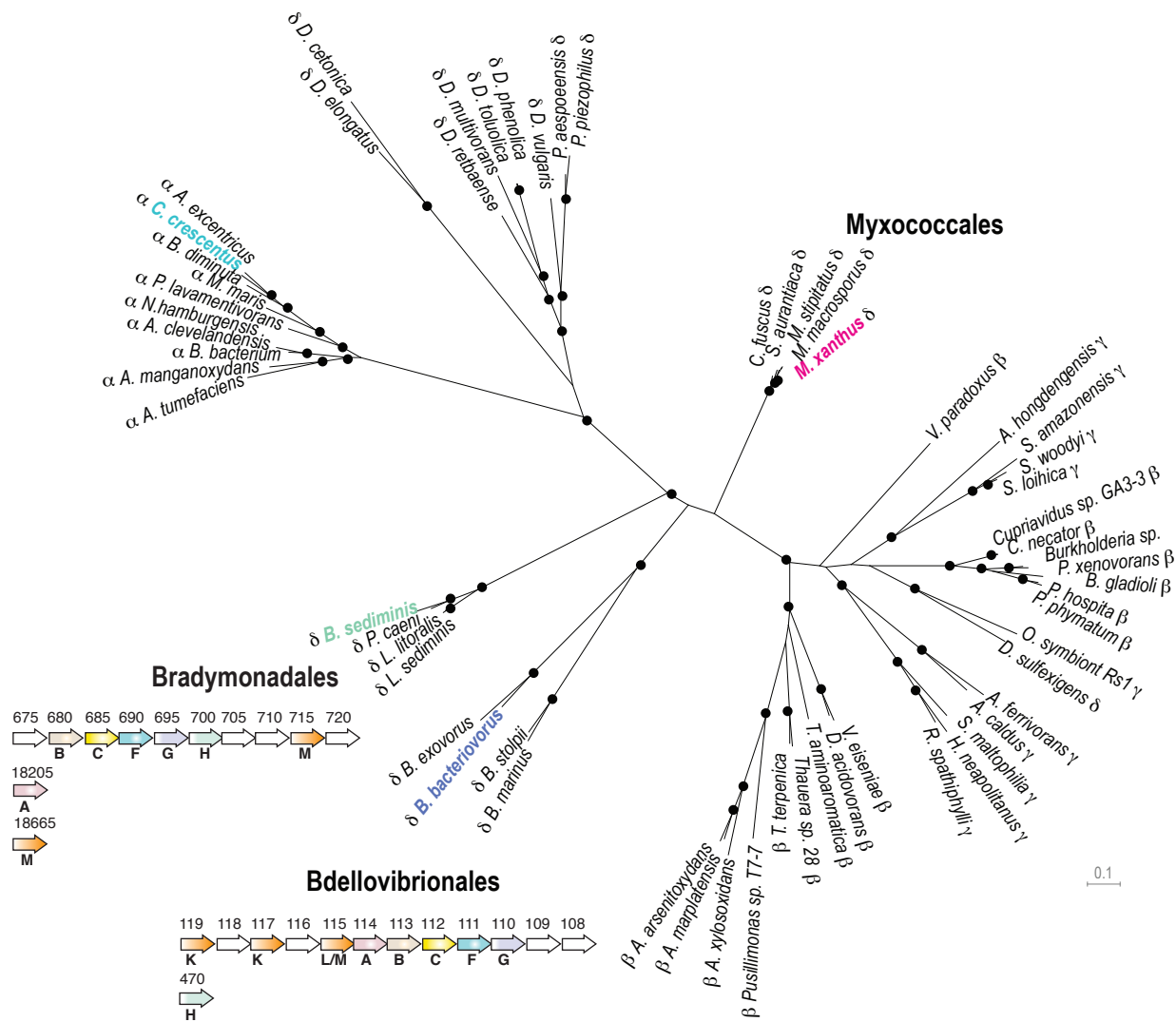


pause

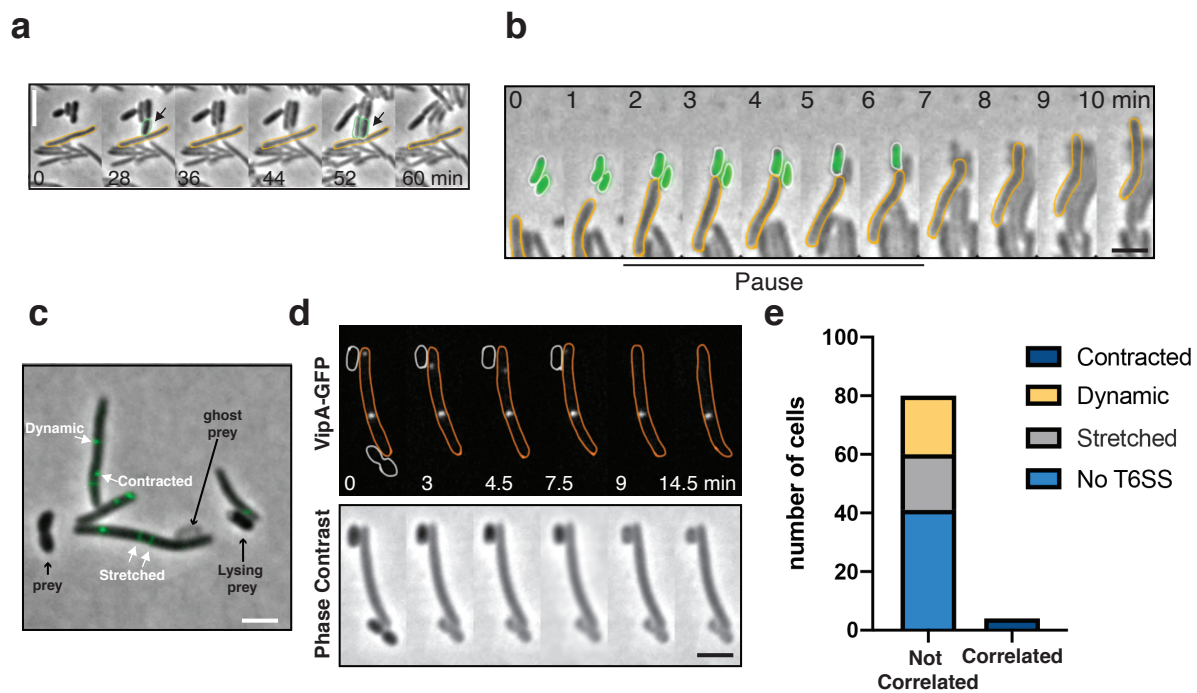


a**b****c****d****e**

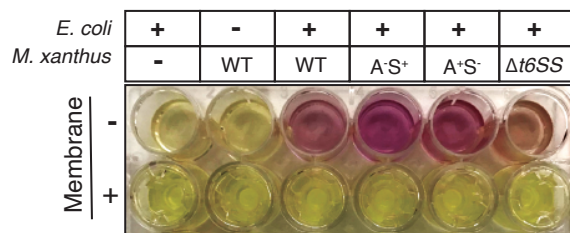




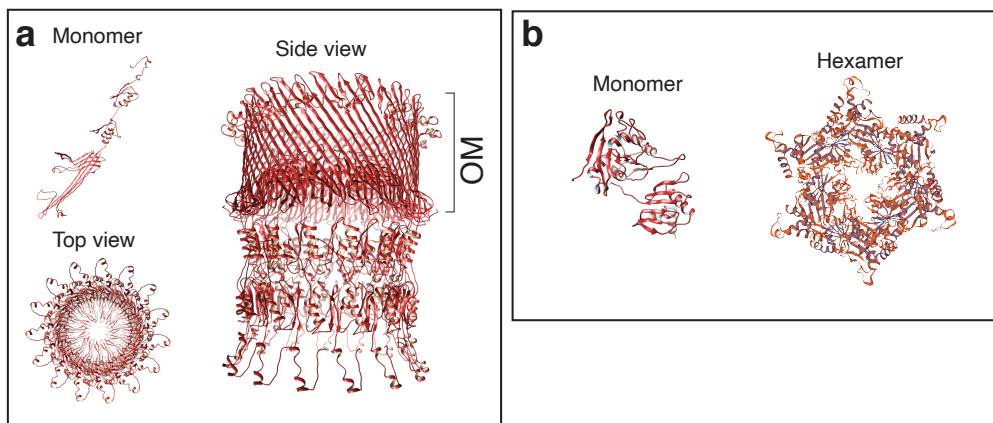
Extended Figure S1



Extended Figure S2



Extended Figure S3



c

G1UBB8 HAEDU -----KFLKNNQGA~~V~~LIEFVFIFFMYSVILIFLIDVAILQATV~~G~~KLQRTSYSLTNVIKERHIERAGDEDI~~K~~EEELKQITKLANLM---
 Q6LP91 PHOPR -----KNRQRGVFAIEMAFVLF~~F~~LCALLTFTGDIAYQLLN~~R~~VNLDRTSYSLVNLKERTFRFFSTQnadgsrtvYAVTQKDDDMET
 U4KGL4 9VIBR -----NLKFRQKGNFSVEFAIVGAFVSLLVFSADVILKISAKGLDRLSYSLVNLKERTQLYGN~~Y~~KITRSEFANAIVIGRNSL---
 Q5E710 VIBF1 -----NLKSRQKGFISIEFAIVGICFSL~~L~~LAFSGDVIKLSIKGLDRLSYSLVNLKERTQLYGMDYQLTSEFVDSLNKIAKNSL---
 TadF Consensus -----rG--avEfalvp-l-----d-----l--aa---a-----l-----

MXAN 4660 EAQEPRAOGASRRSQAAVEAAMIMPLAVFMTLGIIO~~L~~TMMOHAKLMT~~E~~YAA~~Y~~QAARAGI-----VWNGN~~N~~ERMHDA~~A~~IVALLPT
 Mmacrosporus EAQESRAOGASRRSQAAVEAAMIMPLAVFMTLGIIO~~L~~TMMOHAKLMT~~E~~YAA~~Y~~QAARAGI-----VWNGN~~N~~ERMHDA~~A~~IVALLPT
 Mstipitatus E-QEGRSRGTASRQSQAAVEAAMIMPLAVFMTLGIIO~~L~~TLIOHAKLMT~~E~~YAA~~Y~~QAARAGI-----VWNGN~~N~~ERMHDA~~A~~IVALLPT
 Cfuscus -----RESGQAAVESALVLPMLVFLGLIOL~~T~~MQQAKLMT~~E~~YAA~~Y~~CAARTGI-----VWNGN~~N~~ERMHDA~~A~~IVALLPT
 Saurantiaca -----SSGVSRWESGQAAVEAALIMPLMVFMTLGI~~V~~OL~~T~~MIOHAKLMT~~E~~YAA~~Y~~QAARAGS-----VWNGN~~N~~ERMHDA~~A~~IVALLPT

Bd0015 MSRTKFSRTIQNERGMSIAEFIFAIVIAAGLCIVFFALNFTLSMAEIAOYIAFASRAHA-----AGHIDQDKQEOMAKDKYLSL
 M4VDM6 9PROT ---MKRNPRRHNGNSCFIIADFLFAFVMVIGTGIFIFALTFSLATIEVAOYIVWSTARNYS-----AANLNEPAAQQOARQKFENL
 T0RLQ7 9DELT ----RSKHTQISEAQSTIEFLTTFIFAFGFIFLVRLSLSYTNGYL~~V~~H~~Y~~ANVMA~~S~~RTYL-----VFDDNLSN--PIGTDA---
 E1X2R5_HALMS -----MTFVFSFGFIFLFYKISIDATSGFYIHYANFMAARTYL-----TVENNSAN--IAGSDG---

d

B8IRF2 METNO -----GSTAVEFAMVGMIMLV~~T~~MLGIVELGRG~~I~~NVRNQLSQAADFGA-----
 H6RR78 BLASD -----GAAAVEFALV~~V~~LLAVLVLC~~A~~EAFGRAFOTQATLAAARREGA-----
 E9SYB3 RHOHA -----GVAAVEFALV~~V~~PILITLV~~L~~GVIVEFGRGYNQNAVSAARREGA-----
 A1R8Q5 PAEAT -----GAVAVEFALV~~V~~IFLV~~V~~LVLGIFEFGRGFNIQISLSEAAAREAA-----
 TadE Consensus -----G--vE-al--p-l-----aa--aa-----

MXAN 4658 MRARLQMSRS--RGAATVEFALS~~V~~PLLV~~M~~ILMFSMYLTEL~~V~~RAK~~L~~KLOEAA~~R~~YAVWEMTSYALSD~~F~~ANGKHDDAFEDARRFAHKEFVER
 Mmacrosporus MRARLQMSRS--RGAATVEFALS~~V~~PLLV~~M~~ILMFSMYLTEL~~V~~RAK~~L~~KLOEAA~~R~~YAVWEMTSYALSD~~F~~ANGKHDDAFEDARQFAHEPFIER
 Mstipitatus MRTRMSRKSFR--RGGATVEFALS~~V~~PLLV~~M~~ILMFSMYLTEL~~V~~RAK~~L~~KLOEAA~~R~~YAVWEMTSYALTD~~F~~AKGHDDAFEDARKFAHELVVER
 Cfuscus --RANLRTRRRPARRGSS~~T~~VEFAI~~M~~APLLV~~V~~LVLSNYFWEVLRVRIKVAEAA~~R~~FIAFERT--ARKDLG-----QITSEAOQR
 Saurantiaca ----LQFRFR--RGSATVEFAI~~I~~APV~~V~~LMILLF~~S~~MYLTEL~~V~~RAK~~I~~KLOE~~F~~SR~~Y~~AVWEMTSYALSD~~F~~AKAEHDKAFTDAQ~~R~~AMEEATER

Bd0115 TKFSRTIQNE--RCMISAEFIFAIVIAAGLCIVFFALNFTLSMAEIAOYIAFASRAHAAGHIDQ-----DKQEOMAKDKYLS
 M4VDM6 9PROT ---SGFIIADFLFAFVMVIGTGIFIFALTFSLATIEVAOYIVWSTARNYSAANLNE-----PAAQQOARQKFEN
 A0A1J5KI48 9DELT -----MNN-EEGQSTIEFLTTFAFAFSLVFLFIK~~L~~AMNFTNGYLIQYANFMA~~S~~RAYLV~~R~~DTNTPNSVY----TASLTRAREVFNQ
 E1X2R5_HALMS -----MTFVFSFGFIFLFYKISIDATSGFYIHYANFMAARTYLTVENNSANIAGSD----GFAFQQQNVFNS

Extended Figure S4

